

Quasiparticle renormalization and pairing correlations in spherical superfluid nucleiA. Idini,^{1,2} F. Barranco,³ and E. Vigezzi²¹*Dipartimento di Fisica, Università degli Studi di Milano, Via Celoria 16, IT-20133 Milano, Italy*²*INFN, Sezione di Milano, Via Celoria 16, IT-20133 Milano, Italy*³*Departamento de Fisica Aplicada III, Escuela Superior de Ingenieros, Universidad de Sevilla, Camino de los Descubrimientos s/n, ES-41092 Sevilla, Spain*

(Received 25 May 2011; revised manuscript received 15 November 2011; published 31 January 2012)

Within the framework of nuclear field theory (NFT), the spectrum of atomic nuclei is described in terms of collective and quasiparticle degrees of freedom, that is, of elementary modes of excitation that are directly related to experiment and of their coupling, whose strength and form factors are the basic ingredients entering in the calculations of absolute cross sections of inelastic and of one- and two-particle transfer reactions. We present a detailed discussion of the solution of the Dyson equation, also known as the Nambu-Gor'kov equations in the case of a superfluid system, which propagates medium polarization processes calculated making use of NFT to all orders of perturbation, resulting in the dressing of quasiparticles and in the induced pairing interaction. The formalism is applied to the superfluid nucleus ^{120}Sn . Results concerning the low-energy spectrum, that is, the quasiparticle strength distribution of the neighboring odd- A nuclei ^{119}Sn and ^{121}Sn , are presented and compared with the experimental findings.

DOI: [10.1103/PhysRevC.85.014331](https://doi.org/10.1103/PhysRevC.85.014331)

PACS number(s): 21.10.-k, 21.30.Fe, 21.60.Jz

I. INTRODUCTION

Collective and single-particle (quasiparticle) degrees of freedom constitute the elementary modes of nuclear excitation which relate directly to experiment, namely, to the outcome of elastic, inelastic, and one- and two-particle transfer reactions. A central theme in the development of the modern view of nuclear structure has been that of achieving a proper balance in the use of these two apparently contrasting aspects of nuclear dynamics.

The development of nuclear field theory (NFT) (cf., e.g., Ref. [1] and references therein) provided a rigorous theoretical framework to describe nuclear structure in terms of elementary modes of excitation and was instrumental to show that collective and quasiparticle degrees of freedom are not contradictory but complementary facets of nuclear dynamics, as evidenced by their interweaving and by the associated renormalization effects. This is in keeping with the fact that collective and quasiparticle degrees of freedom constitute a basis that is overcomplete: Vibrations and rotations are built of the same quasiparticle degrees of freedom as those involved in independent particle motion. As a consequence, aside from the mean-field and the collective terms, there is a (coupling) term H_C in the NFT Hamiltonian, which is linear in both the single-particle and the collective coordinates. NFT provides the rules to work out, one at a time, the different processes dressing quasiparticle and collective modes. Summing up the different contributions (diagrams) to appropriate order of perturbation, eventually also to infinite order, one can diagonalize H_C and thus renormalize the variety of elementary modes of nuclear excitation. The results of these calculations can be directly compared to experiment, in particular, to effective masses and level densities close to the Fermi energy, as well as to fragmentation of the single-particle strength as observed in one-particle transfer processes. Though these processes have been extensively studied in normal nuclei [2,3], their consequences on pairing correlations have been less investigated.

The basic matrix elements (processes) implied by H_C are those describing the scattering of a quasiparticle from an initial to a final state through the creation of a collective mode. The corresponding form factors and strengths determine the particle-vibration coupling vertex.

A powerful technique to propagate the different lowest-order NFT diagrams such as single-particle and collective vibration dressing processes, as well as induced (phonon-mediated) interactions, in particular, pairing induced interactions, is through Dyson's equation, or, in the case in which the system under consideration is superfluid (superconducting), through the Nambu-Gor'kov equations [4–6]. These equations, which imply the calculation of energy-dependent normal and abnormal self-energies, take into account the pairing interaction induced by the exchange of collective vibrations between members of Cooper pairs and lead to theoretical predictions concerning the low-energy part of the nuclear spectrum; they also produce the structure elements needed for a consistent calculation of one- and two-nucleon transfer reactions [7]. In the present study we extend our previous investigations of medium polarization effects on pairing correlations (cf., in particular, Refs. [8–13]). In Sec. II we provide a detailed account of the formalism, comparing two different schemes for dealing with the Nambu-Gor'kov equations, either solving first the BCS equations with the bare nucleon-nucleon force and then adding renormalization effects (two-step diagonalization; cf. Sec. II A) or dealing at the same time with both sources of pairing (one-step diagonalization; cf. Sec. II B). The coupling between quasiparticle and vibrations is computed according to the basic rules of NFT [14–16] (see also Ref. [17]). Though one is forced to introduce numerical approximations in connection with the calculation of particular quantities and effects, our description contains most of the physics required by the systematic treatment of collective and quasiparticle degrees of freedom and their interweaving as required by NFT. In particular, though we do not consider the coupling of

one- to two-phonon states, essential for the renormalization of the collective degrees of freedom, use is made of empirical collective vibrations, which display the observed collectivity. Within this context, we follow the collective model [16] to calculate the properties of vibrational states in the quasiparticle random phase approximation (QRPA) with a separable force and with a coupling constant chosen so as to reproduce the experimental properties of low-lying collective surface modes.

In most of the computations we use the SLy4 effective interaction, which provides a good reproduction of the overall mean-field properties and which leads, after including renormalization effects, to a sensible single-particle level density around the Fermi energy. Following work carried out in the study of superconductivity in metals use is made of gap equations which generalize the usual BCS expression, allowing one to make contact with other studies. In Sec. III we present results obtained with a self-consistent iterative solution of the Nambu-Gor'kov equations in the case of ^{120}Sn , comparing the theoretical low-lying spectrum of neighboring odd nuclei with experimental data derived from one-neutron transfer reactions. We also compare the results obtained making use of the solution of the Nambu-Gor'kov equations with the quasiparticle approximation. We find that it is possible to separate the contributions to the pairing gap associated with the bare nucleon-nucleon force and with the renormalization effects. The two contributions have comparable magnitudes, in keeping with previous studies. The role played by spin modes, which is known to lead to a repulsive contribution in the pairing 1S_0 channel, whose magnitude in nuclei is very uncertain, is briefly considered, but not discussed in detail. Conclusions are presented in Sec. IV. The sensitivity of our results to various elements of the calculations, is discussed in the Appendix, where we also present a comparison between the one-step and the two-step diagonalization schemes.

II. THE FORMALISM

The objects of our study are pairing correlations in superfluid nuclei taking into account both the contribution of the bare nucleon-nucleon interaction and the many-body effects associated with the coupling between particles and vibrations (cf. Fig. 1).

Our approach is based on two basic assumptions.

- (i) The single-particle basis is obtained making use of a Hartree-Fock (HF) calculation with an effective force.

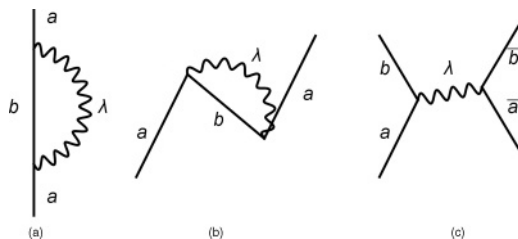


FIG. 1. Basic diagrams taken into account in the present study, which renormalize the normal and abnormal self-energies obtained in mean-field calculations: (a) polarization, (b) correlation, (c) induced pairing interaction, processes.

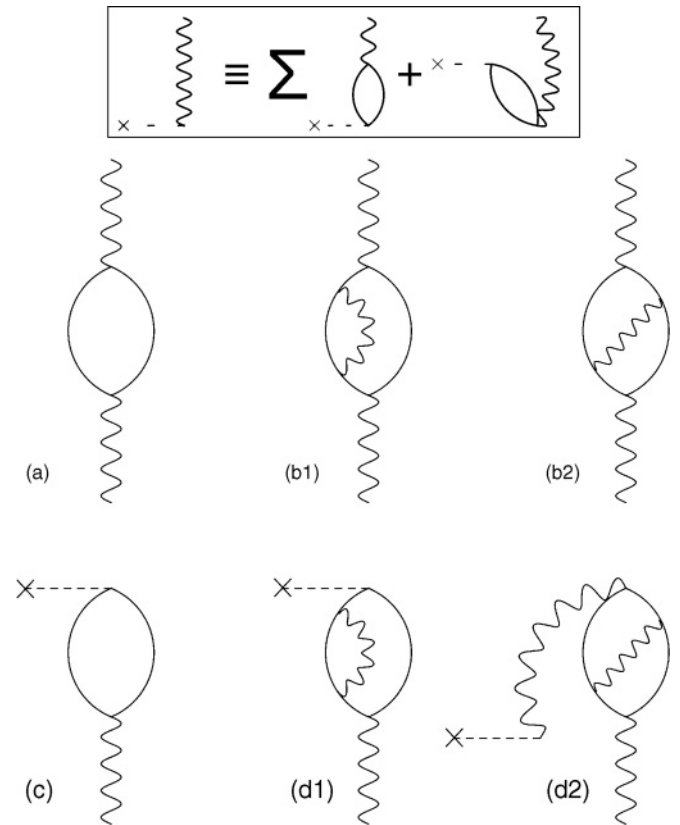


FIG. 2. In NFT the collective vibrational modes are to be calculated in the RPA approximation (see inset and Fig. 6.14 [16]). Consequently, the self-energy graph (a) is, within the framework of NFT, not allowed; neither is any graph that contains any number of bubbles, as they are already considered to infinite order in the collective mode displayed to the left of the identical (\equiv) symbol in the inset. Within this context graph (c) of Fig. 6-11 of Ref. [16] is not allowed. Graphs (b1) and (b2) are the lowest order, particle and vertex renormalization processes of the collective mode displayed in the inset. Similarly, the QRPA transition strength (c) (Tamm-Dancoff contribution) is renormalized by the corresponding diagrams (d1) and (d2).

We have mostly used the SLy4 interaction, mainly because the value of the associated effective mass ($m_k = 0.7m$ in nuclear matter) leads, after renormalization, to a level density in overall agreement with experiment.

- (ii) We do not consider the renormalization processes affecting the vibrations of the system [11,18–20]. The lowest-order diagrams renormalizing the energy of the phonons are shown in Fig. 2(b1) (self-energy correction) and Fig. 2(b2) (vertex correction) while the diagrams shown in Figs. 2(d1) and 2(d2) renormalize the transition strength. The explicit inclusion of renormalization effects on phonons, on par with those on single-particle levels, represents an ambitious program that has been attempted only in a few cases [21–25]. We take the transition densities which are at the basis of the interweaving of single-particle (quasiparticle) degrees of freedom and collective modes from the collective macroscopic Bohr-Mottelson model [16]. We determine the strength of these couplings from a QRPA

calculation adjusted so as to reproduce the experimental properties of the low-lying phonons, using a mean field with an effective mass $m^* = m$ that reproduces the experimental single-particle level density (see Sec. III for more details). In other words, we assume that vertex corrections are effectively included in our couplings. Of course, this is not consistent with the NFT. However, arguably, this represents a reasonable approximation for the renormalization of single-particle properties, as well as for the pairing interaction induced by phonon exchange.

Within this frozen-phonon approximation, as a possible alternative, one can calculate the matrix element $\langle a; \lambda | H_C | b \rangle$ microscopically making use of the transition density of the QRPA phonons obtained from a self-consistent calculation performed with the same effective force employed to obtain the HF mean field. Calculations of this kind have been performed several times in the past for nonsuperfluid nuclei, with various degrees of approximation [2]; see Ref. [26] for a recent calculation aiming at a complete self-consistence. The main drawback in this approach lies in the fact that QRPA leads to a relatively poor reproduction of the experimental energy and the transition strength of the low-lying collective vibrational states in semimagic nuclei (for recent QRPA calculations cf., e.g., [27,28]), which provide the main contribution to renormalization effects of quasiparticle properties. This is consistent with the fact that processes beyond QRPA can strongly renormalize the phonon properties.

The actual implementation of assumptions (i) and (ii) (see above) is presented below in the next sections. Other, less essential assumptions are adopted in our calculation to reduce the computational complexity. First of all, we limit the investigation of renormalization processes to states lying close to the Fermi energy. We then take into account the fact that the bare interaction, even considering its soft-core or $V_{\text{low}k}$ versions, couples the single-particle states lying close to the Fermi energy with states lying up to several hundreds of MeV, while the phonon-mediated pairing interaction acts between

pairs of states separated by a few MeV [12,29]. This suggests the convenience of a separate treatment of the two interactions in the pairing problem by performing a HF + BCS calculation prior to the calculation of many-body effects. We refer to this approach as the two-step diagonalization scheme. Otherwise, one is forced to consider the bare and the induced interaction on the same footing (one-step diagonalization). In the following we first illustrate in detail the two-step scheme, which is used in most calculations presented in this paper. We then outline the main modifications involved in the one-step diagonalization scheme.

A. Two-step diagonalization scheme

A convenient formalism for the calculation of the properties of quasiparticles in superfluid nuclei within the two-step diagonalization scheme was given by Van der Sluys *et al.* [30], although they did not devote particular attention to the renormalization of pairing correlations. In this approach one first accounts for the action of the bare force with a HF + BCS calculation, discussed in more detail in Sec. III A1, leading to quasiparticle energies E_a , quasiparticles amplitudes u_a and v_a , and to a pairing gap Δ_a^{BCS} . One then renormalizes the obtained quasiparticles including the coupling to vibrations calculated in the QRPA. The derivation of the formalism was based on the equation-of-motion method, which has a very close relation to the Green's functions formalism used to derive the Nambu-Gor'kov equations, commonly used to study superconductivity in condensed-matter physics [31].

To calculate the renormalization of a quasiparticle in spherical nuclei, denoted by its associated quantum numbers $a \equiv \{nlj\}$, one has to solve a system of linear equations obtained coupling the quasiparticle with more complex configurations including phonon states (see Fig. 1). The phonons are characterized by their angular momentum λ and by their energy $\hbar\omega_{\lambda,\nu}$. We assume that phonons have natural parity, $\pi = (-1)^\lambda$ (see, however, Sec. III A3). For illustration, we write the diagonalization problem including only two other quasiparticle states b and c , and a single phonon λ, ν :

$$\begin{pmatrix} E_a & V(ab\lambda\nu) & V(ac\lambda\nu) & W(ab\lambda\nu) & W(ac\lambda\nu) & 0 \\ V(ab\lambda\nu) & \hbar\omega_{\lambda\nu} + E_b & 0 & 0 & 0 & W(ab\lambda\nu) \\ V(ac\lambda\nu) & 0 & \hbar\omega_{\lambda\nu} + E_c & 0 & 0 & W(ac\lambda\nu) \\ W(ab\lambda\nu) & 0 & 0 & -\hbar\omega_{\lambda\nu} - E_b & 0 & -V(ab\lambda\nu) \\ W(ac\lambda\nu) & 0 & 0 & 0 & -\hbar\omega_{\lambda\nu} - E_c & -V(ac\lambda\nu) \\ 0 & W(ab\lambda\nu) & W(ac\lambda\nu) & -V(ab\lambda\nu) & -V(ac\lambda\nu) & -E_a \end{pmatrix} \begin{pmatrix} x_{a(n)} \\ C_{a(n),b,\lambda\nu} \\ C_{a(n),c,\lambda\nu} \\ -D_{a(n),b,\lambda\nu} \\ -D_{a(n),c,\lambda\nu} \\ -y_{a(n)} \end{pmatrix},$$

$$= \tilde{E}_{a(n)} \begin{pmatrix} x_{a(n)} \\ C_{a(n),b,\lambda\nu} \\ C_{a(n),c,\lambda\nu} \\ -D_{a(n),b,\lambda\nu} \\ -D_{a(n),c,\lambda\nu} \\ -y_{a(n)} \end{pmatrix}.$$
(1)

Many eigenvalues $\tilde{E}_{a(n)}$ and eigenstates $a(n)$ are obtained from the diagonalization of the matrix (1), giving rise to a fragmentation of the associated quasiparticle strength. For a given eigenvalue $\tilde{E}_{a(n)} > 0$ there exists a corresponding eigenvalue $\tilde{E}_{a(-n)} = -\tilde{E}_{a(n)}$. As in standard BCS theory, we keep only positive energy solutions, $n > 0$.

The amplitudes obey the normalization condition

$$x_{a(n)}^2 + \sum_{b,\lambda,\nu} [C_{a(n),b,\lambda\nu}^2] + y_{a(n)}^2 + \sum_{b,\lambda,\nu} [D_{a(n),b,\lambda\nu}^2] = 1, \quad (2)$$

$C_{a(n),b,\lambda\nu}$ and $-D_{a(n),b,\lambda\nu}$ being the components on the complex $1qp \otimes 1ph$ states $\alpha_b^\dagger \Gamma_{\lambda\nu}^\dagger$ and $\alpha_{\bar{b}} \Gamma_{\lambda\bar{\nu}}$, while $x_{a(n)}$ and $-y_{a(n)}$ are the components on the original $1qp$ states α_a^\dagger and $\alpha_{\bar{a}}$, where \bar{a} denotes the time-reversed state. The fragment $a(n)$ carries a fraction of the strength

$$N_{a(n)} = x_{a(n)}^2 + y_{a(n)}^2 < 1, \quad (3)$$

which is to be compared with the experimental quasiparticle strength, as determined, for example, in one-particle-transfer reactions.

The excitation operator derived from Eq. (1),

$$\tilde{O}_{a(n)}^\dagger = \tilde{\alpha}_{a(n)qp}^\dagger + C_{a(n),b,\lambda\nu} \alpha_b^\dagger \Gamma_{\lambda\nu}^\dagger - D_{a(n),b,\lambda\nu} \alpha_{\bar{b}} \Gamma_{\lambda\bar{\nu}}$$

contains the quasiparticle component

$$\tilde{\alpha}_{a(n)qp}^\dagger = x_{a(n)} \alpha_a^\dagger - y_{a(n)} \alpha_{\bar{a}}.$$

Taking into account the BCS Bogoliubov transformation,

$$\alpha_a^\dagger = u_a a_a^\dagger + v_a a_{\bar{a}},$$

one can write

$$\tilde{\alpha}_{a(n)qp}^\dagger = \tilde{u}_{a(n)} a_a^\dagger + \tilde{v}_{a(n)} a_{\bar{a}},$$

where the quantities

$$\begin{aligned} \tilde{u}_{a(n)} &= x_{a(n)} u_a - y_{a(n)} v_a, \\ \tilde{v}_{a(n)} &= x_{a(n)} v_a + y_{a(n)} u_a, \end{aligned} \quad (4)$$

represent the new quasiparticle amplitudes associated with a given fragment $a(n)$: Their squares give the spectroscopic factors associated with one-nucleon transfer reactions.

We can then calculate the renormalized pairing gap as [cf. below Eq. (38)]

$$\tilde{\Delta}_{a(n)} = \frac{2\tilde{E}_{a(n)} \tilde{u}_{a(n)} \tilde{v}_{a(n)}}{\tilde{u}_{a(n)}^2 + \tilde{v}_{a(n)}^2}. \quad (5)$$

The quasiparticle-phonon matrix elements $V(ab\lambda\nu)$ and $W(ab\lambda\nu)$ in Eq. (1) are given by

$$\begin{aligned} V(ab\lambda\nu) &= \left[\frac{2\lambda + 1}{2j_a + 1} \right]^{1/2} \sum_{c \leq d} (1 + \delta_{cd})^{-1/2} \\ &\times [X_{cd}(\lambda\nu) V(cd\lambda b; a) + (-1)^{j_a - j_b + \lambda} \\ &\times Y_{cd}(\lambda\nu) V(cd\lambda a; b)] \end{aligned} \quad (6)$$

and

$$\begin{aligned} W(ab\lambda\nu) &= \left[\frac{2\lambda + 1}{2j_a + 1} \right]^{1/2} \sum_{c \leq d} (1 + \delta_{cd})^{-1/2} \\ &\times [X_{cd}(\lambda\nu) R(abcd; \lambda) + Y_{cd}(\lambda\nu) Q(abcd; \lambda)], \end{aligned} \quad (7)$$

where X_{cd} and Y_{cd} are the forward and backward amplitudes resulting from the QRPA calculation.

The terms $V(cd\lambda b; a)$, $Q(abcd; \lambda)$ and $R(abcd; \lambda)$ are given by

$$\begin{aligned} V(cd\lambda b; a) &= -(u_a v_b u_c u_d - v_a u_b v_c v_d) G(abcd\lambda) \\ &+ (u_a u_b u_c v_d - v_a v_b v_c u_d) F(abcd\lambda) \\ &+ (-1)^{j_c - j_d + \lambda} (u_a u_b v_c u_d - v_a v_b u_c v_d) \\ &\times F(abdc\lambda), \end{aligned} \quad (8)$$

$$\begin{aligned} Q(abcd; \lambda) &= (u_a u_b u_c u_d + v_a v_b v_c v_d) G(abcd\lambda) \\ &+ (u_a v_b u_c v_d + v_a u_b v_c u_d) F(abcd\lambda) \\ &+ (-1)^{j_c - j_d + \lambda} (u_a v_b v_c u_d + v_a u_b u_c v_d) \\ &\times F(abdc\lambda), \end{aligned} \quad (9)$$

$$\begin{aligned} R(abcd; \lambda) &= -(u_a u_b v_c v_d + v_a v_b u_c u_d) G(abcd\lambda) \\ &+ (u_a v_b v_c u_d + v_a u_b u_c v_d) F(abcd\lambda) \\ &+ (-1)^{j_c - j_d + \lambda} (u_a v_b u_c v_d + v_a u_b v_c u_d) \\ &\times F(abdc\lambda), \end{aligned} \quad (10)$$

where $F(abcd\lambda)$ and $G(abcd\lambda)$ denote the angular momentum coupled antisymmetrized particle-hole and particle-particle $\langle ab\lambda | V | cd\lambda \rangle_{as}$ matrix element, respectively. Note that in the limit of nonsuperfluid nuclei (all u, v terms equal to 0 or 1), the matrix elements $V(ab\lambda\nu)$ connect pairs of states a, b above or below the Fermi energy through the F terms and pairs of states on opposite parts of the Fermi energy through the G terms, though the opposite is true for the $W(ab\lambda\nu)$ matrix elements. In the following we do not take into account the coupling with pair vibration modes, neglecting the G terms in Eqs. (8)–(10). While this coupling is known to be relevant for closed-shell nuclei, it is expected to be much less important for the superfluid case, because most of the two-particle transfer strength is already incorporated in the BCS ground-state (gauge space deformed) wave function [32].

The F and G matrix elements were obtained in [30] from a calculation performed using the same force adopted in the HF + BCS calculations. In our approach, the QRPA calculation is instead decoupled from the renormalization process, in keeping with the main assumption (ii) discussed above. In our QRPA calculation we use the separable force

$$V(\vec{r}_1, \vec{r}_2) = -\kappa_{\text{self}} r_1 \frac{\partial U}{\partial r_1} r_2 \frac{\partial U}{\partial r_2} \sum_{\lambda\mu} \chi_\lambda Y_{\lambda\mu}^*(\theta_1) Y_{\lambda\mu}(\theta_2), \quad (11)$$

where $U(r)$ is a potential that gives a good reproduction of the experimental single-particle levels. In practice, we adopt the Woods-Saxon parametrization given in Ref. [33] [cf. Eq. (2-182)] together with an empirical pairing coupling constant adjusted to reproduce the pairing gap deduced from the experimental odd-even mass difference. The parameters χ_λ are determined so as to get a good agreement with the observed properties (energy and transition strength) of the low-lying surface modes. More precisely, we reproduce the polarizability $\beta_{\lambda 1}^2 / \hbar \omega_{\lambda 1}$ of the low-lying modes, where $\beta_{\lambda\nu}$ denotes the experimental nuclear deformation parameter. In fact, the matrix elements of the phonon-induced pairing interaction for levels close to the Fermi energy are approximately proportional

to the polarizability of the mode [cf. Eq. (30) below]. The resulting values of χ_λ turn out to be close to 1 (cf. Sec. III), indicating that the QRPA coupling constant is close to the Bohr-Mottelson self-consistent coupling constant $\kappa_{\text{self}} = -[\int r \frac{\partial \rho}{\partial r} r \frac{\partial U}{\partial r} r^2 dr]^{-1}$.

This scheme is the coupling scheme given by Bohr and Mottelson [16] [cf. Eqs. (6-207)–(6-209)]. The particle-hole matrix elements, neglecting the exchange terms [cf. on this point Ref. [34], Eq. (14.54) and Chap. 16], are given by

$$F(abcd\lambda) = -\kappa_{\text{self}} \chi_\lambda \langle ab\lambda\mu | r_1 \frac{\partial U}{\partial r_1} Y_{\lambda\mu}^*(\theta_1) | 0 \rangle \langle 0 | r_2 \frac{\partial U}{\partial r_2} Y_{\lambda\mu}^*(\theta_2) | cd\lambda\mu \rangle, \quad (12)$$

where μ is any of the z projections of the angular momentum λ . In this expression the QRPA-like single-particle indices (c, d) and the scattered particle indices (a, b) appear in separated factors, so that one gets the angular momentum reordering property $F(abdc\lambda) = (-1)^{j_c - j_a + \lambda} F(abcd\lambda) = (-1)^{j_a - j_b + \lambda} F(bacd\lambda)$ and

$$V(ab\lambda\nu) = -\kappa_{\text{self}} \chi_\lambda (u_a u_b - v_a v_b) \langle ab\lambda\mu | r_1 \frac{\partial U}{\partial r_1} Y_{\lambda\mu}^*(\theta_1) | 0 \rangle \left[\frac{2\lambda + 1}{2j_a + 1} \right]^{1/2} \times \sum_{c \leq d} (1 + \delta_{cd})^{-1/2} \left\{ [X_{cd}(\lambda\nu) + Y_{cd}(\lambda\nu)] (u_c v_d + v_c v_d) \langle 0 | r_2 \frac{\partial U}{\partial r_2} Y_{\lambda\mu}^*(\theta_2) | cd\lambda\mu \rangle \right\}. \quad (13)$$

The quantity in the summation is precisely the transition amplitude $M(\lambda\nu)$ of the $\hat{M} = r_2 \frac{\partial U}{\partial r_2} Y_{\lambda\mu}^*(\theta_2)$ operator, which is usually expressed in terms of the so-called collective deformation parameter as $M(\lambda\nu) = \alpha_{\lambda\nu}^o / \kappa_{\text{self}}$, assuming a collectively deformed density $\delta\rho = -r \frac{\partial \rho}{\partial r} \sum_{\lambda\mu} Y_{\lambda\mu}^*(\theta) \alpha_{\lambda\mu}$, where $\alpha_{\lambda\mu} = i^{-\lambda} \alpha_{\lambda\nu}^o [\Gamma_{\lambda\mu}^\dagger + (-1)^\mu \Gamma_{\lambda-\mu}]_v$.

In this way we can write

$$V(ab\lambda\nu) = -\chi_\lambda (u_a u_b - v_a v_b) \langle ab\lambda\mu | r_1 \frac{\partial U}{\partial r_1} Y_{\lambda\mu}^*(\theta_1) | 0 \rangle \left[\frac{2\lambda + 1}{2j_a + 1} \right]^{1/2} \alpha_{\lambda\nu}^o. \quad (14)$$

Finally, following the notation in Ref. [16], Eqs. (6-207)–(6-209) using the reduced matrix element $\langle j_b || Y_\lambda || j_a \rangle = (-1)^{j_a - j_b} \langle j_a j_b; \lambda\mu | Y_{\lambda\mu} | 0 \rangle \sqrt{2\lambda + 1}$ and the relation $\alpha_{\lambda\nu}^o = \beta_{\lambda\nu} / \sqrt{2\lambda + 1}$, we can write

$$V(ab\lambda\nu) = h(ab\lambda\nu) (u_a u_b - v_a v_b), \quad (15)$$

where

$$h(ab\lambda\nu) = -(-1)^{j_a - j_b} \beta_{\lambda\nu}^{\text{eff}} \langle a | r_1 \frac{\partial U}{\partial r_1} | b \rangle \times \langle j_b || Y_\lambda || j_a \rangle \left[\frac{1}{(2j_a + 1)(2\lambda + 1)} \right]^{1/2}, \quad (16)$$

which is the basic vertex in Ref. [16] corrected by an effective deformation parameter $\beta_{\lambda\nu}^{\text{eff}} = \chi_\lambda \beta_{\lambda\nu}$.

Analogously, one finds

$$W(ab\lambda\nu) = h(ab\lambda\nu) (u_a v_b + v_a u_b). \quad (17)$$

A self-consistent renormalization procedure is then carried out by iterating the diagonalization process, using the previously renormalized quasiparticles to build the complex

$1qp \otimes 1ph$ states. This means that the basic V, W matrix elements are now calculated as

$$\begin{aligned} V(ab(m)\lambda\nu) &= h(ab\lambda\nu) (u_a \tilde{u}_{b(m)} - v_a \tilde{v}_{b(m)}), \\ W(ab(m)\lambda\nu) &= h(ab\lambda\nu) (u_a \tilde{v}_{b(m)} + v_a \tilde{u}_{b(m)}), \end{aligned} \quad (18)$$

where the u_a and v_a amplitudes obtained from the initial HF + BCS calculation are kept fixed in the iteration process, while $\tilde{u}_{b(m)}$ and $\tilde{v}_{b(m)}$ refer to the amplitudes associated with the m fragment resulting from the renormalization of the state b in the previous iteration step. In this way a consistent fragmentation of the different states is constructed through the iterative procedure.

The iteration process gives rise to the so-called no-line crossing rainbow series of the self-energy (see below), in which all orders are summed up coherently and which is expected to play an important role in the limit of strong coupling (cf. Fig. 3). The size of the matrix to be diagonalized increases exponentially at each iteration, and some sort of numerical approximation is needed, as is discussed in Sec. III.



FIG. 3. The coupling of the quasiparticle to many-phonon states, corresponding to the rainbow diagrams shown in the figure, is included in our approach through the iteration of the self-consistent diagonalization of the Nambu-Gor'kov matrix.

1. Energy-dependent, BCS-like formulation

Projecting onto the $1qp$ -particle space, the diagonalization of the eigenvalue problem (1) can be written as a 2×2 energy-dependent eigenvalue problem, which is equivalent to that derived from an approach based on Green's function formalism (cf., e.g., Ref. [9]):

$$\begin{pmatrix} E_a + \Sigma_{a(n)}^{11\text{pho}} & \Sigma_{a(n)}^{12\text{pho}} \\ \Sigma_{a(n)}^{12\text{pho}} & -E_a + \Sigma_{a(n)}^{22\text{pho}} \end{pmatrix} \begin{pmatrix} x_{a(n)} \\ y_{a(n)} \end{pmatrix} = \tilde{E}_{a(n)} \begin{pmatrix} x_{a(n)} \\ y_{a(n)} \end{pmatrix}, \quad (19)$$

where one has introduced the energy-dependent, normal self-energies $\Sigma_{a(n)}^{11\text{pho}}$ and $\Sigma_{a(n)}^{22\text{pho}}$ given by

$$\begin{aligned} \Sigma_{a(n)}^{11\text{pho}} &= \sum_{b,m,\lambda,\nu} \frac{V^2[ab(m)\lambda\nu]}{\tilde{E}_{a(n)} - \tilde{E}_{b(m)} - \hbar\omega_{\lambda\nu}} \\ &+ \sum_{b,m,\lambda,\nu} \frac{W^2[ab(m)\lambda\nu]}{\tilde{E}_{a(n)} + \tilde{E}_{b(m)} + \hbar\omega_{\lambda\nu}}, \\ \Sigma_{a(n)}^{22\text{pho}} &= \sum_{b,m,\lambda,\nu} \frac{W^2[ab(m)\lambda\nu]}{\tilde{E}_{a(n)} - \tilde{E}_{b(m)} - \hbar\omega_{\lambda\nu}} \\ &+ \sum_{b,m,\lambda,\nu} \frac{V^2[ab(m)\lambda\nu]}{\tilde{E}_{a(n)} + \tilde{E}_{b(m)} + \hbar\omega_{\lambda\nu}}, \end{aligned} \quad (20)$$

and the abnormal self-energy,

$$\begin{aligned} \Sigma_{a(n)}^{12\text{pho}} &= - \sum_{b,m,\lambda,\nu} V[ab(m)\lambda\nu]W[ab(m)\lambda\nu] \\ &\times \left[\frac{1}{\tilde{E}_{a(n)} - \tilde{E}_{b(m)} - \hbar\omega_{\lambda\nu}} \right. \\ &\left. - \frac{1}{\tilde{E}_{a(n)} + \tilde{E}_{b(m)} + \hbar\omega_{\lambda\nu}} \right]. \end{aligned} \quad (21)$$

We note that Σ^{11} evaluated at a given energy E is equal to $-\Sigma^{22}$ evaluated at $-E$, that is, $\Sigma_{a(n)}^{11\text{pho}} = -\Sigma_{a(-n)}^{22\text{pho}}$. The normalization of the quasiparticle strength of the n fragment [cf. Eq. (2)] is given by [35]

$$\begin{aligned} x_{a(n)}^2 + y_{a(n)}^2 - \frac{\partial \Sigma_{a(n)}^{11\text{pho}}}{\partial \tilde{E}_{a(n)}} x_{a(n)}^2 - \frac{\partial \Sigma_{a(n)}^{22\text{pho}}}{\partial \tilde{E}_{a(n)}} y_{a(n)}^2 \\ - 2 \frac{\partial \Sigma_{a(n)}^{12\text{pho}}}{\partial \tilde{E}_{a(n)}} x_{a(n)} y_{a(n)} = 1. \end{aligned} \quad (22)$$

In this form one can easily make contact with the formalism based on the Green's function for superfluid systems,

$$\hat{G}_a(\tilde{E}_a + i\delta) = [(\tilde{E}_a + i\delta)\mathbf{1} - E_a\tau_3 - \hat{\Sigma}_a^{\text{pho}}(\tilde{E}_a + i\delta)]^{-1}, \quad (23)$$

where τ_3 denotes a Pauli matrix and where

$$\begin{aligned} \hat{\Sigma}_a^{\text{pho}}(\tilde{E}_a + i\delta) \\ = \begin{pmatrix} \Sigma_a^{11\text{pho}}(\tilde{E}_a + i\delta) & \Sigma_a^{12\text{pho}}(\tilde{E}_a + i\delta) \\ \Sigma_a^{12\text{pho}}(\tilde{E}_a + i\delta) & \Sigma_a^{22\text{pho}}(\tilde{E}_a + i\delta) \end{pmatrix} \end{aligned} \quad (24)$$

is our phonon-mediated self-energy matrix evaluated at the complex energy $\tilde{E}_a + i\delta$, which coincides with the matrix

introduced by Nambu and extensively used in condensed matter to deal with strong coupling superconductivity [31]. Equations (23) and (24) must be solved self-consistently owing to the fact that the quasiparticle strengths needed for the evaluation of $\hat{\Sigma}_a^{\text{pho}}(\tilde{E}_a + i\delta)$ through the V and W matrix elements are obtained from the imaginary part of $\hat{G}_a(E + i\delta)$ [cf. Ref. [30], Eqs. (46) and (47)].

To get more insight concerning the respective contributions of the bare and of the phonon-induced interaction to the pairing gap, it is useful to rewrite the 2×2 eigenvalue problem (19) in terms of the amplitudes \tilde{u} , \tilde{v} , instead of x , y , by inverting the relation (4), obtaining

$$\begin{pmatrix} (\epsilon_a - \epsilon_F) + \tilde{\Sigma}_{a(n)}^{11} & \tilde{\Sigma}_{a(n)}^{12} \\ \tilde{\Sigma}_{a(n)}^{12} & -(\epsilon_a - \epsilon_F) + \tilde{\Sigma}_{a(n)}^{22} \end{pmatrix} \begin{pmatrix} \tilde{u}_{a(n)} \\ \tilde{v}_{a(n)} \end{pmatrix} = \tilde{E}_{a(n)} \begin{pmatrix} \tilde{u}_{a(n)} \\ \tilde{v}_{a(n)} \end{pmatrix}, \quad (25)$$

where ϵ_a denotes the HF single-particle energy, while the new normal self-energies are given by

$$\begin{aligned} \tilde{\Sigma}_{a(n)}^{11} &= u_a^2 \Sigma_{a(n)}^{11\text{pho}} + v_a^2 \Sigma_{a(n)}^{22\text{pho}} - 2u_a v_a \Sigma_{a(n)}^{12\text{pho}} \\ \tilde{\Sigma}_{a(n)}^{22} &= u_a^2 \Sigma_{a(n)}^{22\text{pho}} + v_a^2 \Sigma_{a(n)}^{11\text{pho}} + 2u_a v_a \Sigma_{a(n)}^{12\text{pho}}. \end{aligned} \quad (26)$$

One can separate the abnormal self-energy into two terms, writing

$$\tilde{\Sigma}_{a(n)}^{12} = \Delta_a^{\text{BCS}} + \tilde{\Sigma}_{a(n)}^{12,\text{pho}}. \quad (27)$$

The first term, Δ_a^{BCS} , is the pairing gap associated with the bare interaction obtained in the HF + BCS calculation, while the second term is associated with the phonon-induced interaction and is given by

$$\tilde{\Sigma}_{a(n)}^{12,\text{pho}} = \Sigma_{a(n)}^{12\text{pho}} (u_a^2 - v_a^2) + u_a v_a (\Sigma_{a(n)}^{11\text{pho}} - \Sigma_{a(n)}^{22\text{pho}}). \quad (28)$$

Using Eqs. (18), (20), and (21) this expression can be simplified and the abnormal self-energy can be rewritten as

$$\tilde{\Sigma}_{a(n)}^{12,\text{pho}} = - \sum_{b,m} \frac{(2j_b + 1)}{2} V_{\text{ind}}[a(n)b(m)] \tilde{u}_{b(m)} \tilde{v}_{b(m)}, \quad (29)$$

where we have introduced the induced pairing interaction:

$$\begin{aligned} V_{\text{ind}}[a(n)b(m)] &= \sum_{\lambda,\nu} \frac{2h^2(ab\lambda\nu)}{(2j_b + 1)} \left[\frac{1}{\tilde{E}_{a(n)} - \tilde{E}_{b(m)} - \hbar\omega_{\lambda\nu}} \right. \\ &\left. - \frac{1}{\tilde{E}_{a(n)} + \tilde{E}_{b(m)} + \hbar\omega_{\lambda\nu}} \right]. \end{aligned} \quad (30)$$

Furthermore, we can symmetrize the matrix (25) to get a 2×2 eigenvalue equation which is formally identical to the BCS eigenvalue equation. This can be achieved multiplying Eq. (25) by the $Z_{a(n)}$ energy-dependent function,

$$Z_{a(n)} = \left(1 - \frac{\tilde{\Sigma}_{a(n)}^{\text{odd}}}{\tilde{E}_{a(n)}} \right)^{-1}, \quad (31)$$

where $\tilde{\Sigma}^{\text{odd}}$ is the odd part of $\tilde{\Sigma}_{a(n)}^{11}$

$$\tilde{\Sigma}_{a(n)}^{\text{odd}} = \frac{\tilde{\Sigma}_{a(n)}^{11} + \tilde{\Sigma}_{a(n)}^{22}}{2} = \frac{\Sigma_{a(n)}^{11\text{pho}} + \Sigma_{a(n)}^{22\text{pho}}}{2}. \quad (32)$$

We note that according to the definition above, Z is the inverse of the correspondent quantity as defined in Refs. [9] and [31]. We also note that the symbol Z is often used instead of N to define the quasiparticle strength. In fact, the two quantities tend to take similar values close to the Fermi energy (cf. Fig. 7 below). This similarity can be explained by noting that for the lowest pole, the finite difference in the expression of Z can be approximated by a derivative:

$$Z_{a(n)} = \left(1 - \frac{\Sigma_{a(n)}^{11} - \Sigma_{a(-n)}^{11}}{2\tilde{E}_{a(n)}} \right)^{-1} \approx \left(1 - \frac{\partial \Sigma_{a(n)}^{11}}{\partial \tilde{E}_{a(n)}} \right)^{-1}. \quad (33)$$

Furthermore, in the normalization of the strength of quasiparticles close to the Fermi energy, $x \gg y$ so that, using Eq. (22),

$$N_{a(n)} = x_{a(n)}^2 + y_{a(n)}^2 \approx x_{a(n)}^2 \approx \left(1 - \frac{\partial \Sigma_{a(n)}^{11}}{\partial \tilde{E}_{a(n)}} \right)^{-1}. \quad (34)$$

Having multiplied by $Z_{a(n)}$, it is possible to rewrite Eq. (25) as

$$\begin{pmatrix} \tilde{\epsilon}_{a(n)} - \epsilon_F & \tilde{\Delta}_{a(n)} \\ \tilde{\Delta}_{a(n)} & -(\tilde{\epsilon}_{a(n)} - \epsilon_F) \end{pmatrix} \begin{pmatrix} \tilde{u}_{a(n)} \\ \tilde{v}_{a(n)} \end{pmatrix} = \tilde{E}_{a(n)} \begin{pmatrix} \tilde{u}_{a(n)} \\ \tilde{v}_{a(n)} \end{pmatrix}, \quad (35)$$

where

$$\tilde{\epsilon}_{a(n)} - \epsilon_F = Z_{a(n)} [(\epsilon_a - \epsilon_F) + \tilde{\Sigma}_{a(n)}^{\text{even}}], \quad (36)$$

and where $\tilde{\Sigma}_{a(n)}^{\text{even}}$ is the even part of $\tilde{\Sigma}_{a(n)}^{11}$:

$$\begin{aligned} \tilde{\Sigma}_{a(n)}^{\text{even}} &= \frac{\tilde{\Sigma}_{a(n)}^{11} - \tilde{\Sigma}_{a(n)}^{22}}{2} = (u_a^2 - v_a^2) \frac{\Sigma_{a(n)}^{1\text{pho}} - \Sigma_{a(n)}^{22\text{pho}}}{2} \\ &\quad - 2u_a v_a \Sigma_{a(n)}^{12\text{pho}}. \end{aligned} \quad (37)$$

The term $\tilde{\epsilon}_{a(n)}$ in Eq. (35) represents the renormalized single-particle energy, and one can now identify the pairing gap with the term $\tilde{\Delta}_{a(n)}$ [31]:

$$\begin{aligned} \tilde{\Delta}_{a(n)} &= Z_{a(n)} \tilde{\Sigma}_{a(n)}^{12} \\ &= Z_{a(n)} \left(\Delta_a^{\text{BCS}} + \tilde{\Sigma}_{a(n)}^{12,\text{pho}} \right) \equiv \tilde{\Delta}_{a(n)}^{\text{bare}} + \tilde{\Delta}_{a(n)}^{\text{pho}}. \end{aligned} \quad (38)$$

On the other hand, eliminating $\tilde{\epsilon}_{a(n)} - \epsilon_F$ from Eq. (35), one obtains the expression (5) introduced above, which can be used when solving the energy-independent problem (1), because it involves only quasiparticle energies and amplitudes. Note also that the quasiparticle energy relates to the new gap and single-particle energy as in the usual BCS equations:

$$\tilde{E}_{a(n)} = \sqrt{(\tilde{\epsilon}_{a(n)} - \epsilon_F)^2 + \tilde{\Delta}_{a(n)}^2} \quad (39)$$

It is now possible to write a generalized gap equation. Introducing the total quasiparticle strength for a given fragment,

$$\tilde{u}_{a_n}^2 + \tilde{v}_{a_n}^2 = N_{a(n)}, \quad (40)$$

the product $\tilde{u}_{a(n)}\tilde{v}_{a(n)}$ may be obtained in the usual way from the 2×2 secular equation as

$$\tilde{u}_{a(n)}\tilde{v}_{a(n)} = N_{a(n)} \frac{\tilde{\Delta}_{a(n)}}{2\sqrt{(\tilde{\epsilon}_{a(n)} - \epsilon_F)^2 + \tilde{\Delta}_{a(n)}^2}}, \quad (41)$$

or, equivalently, by using Eqs. (37) and (38), as

$$\tilde{u}_{a(n)}\tilde{v}_{a(n)} = N_{a(n)} \frac{Z_{a(n)} \tilde{\Sigma}_{a(n)}^{12}}{2\sqrt{Z_{a(n)}^2 (\epsilon_a - \epsilon_F + \tilde{\Sigma}_{a(n)}^{\text{even}})^2 + (Z_{a(n)} \tilde{\Sigma}_{a(n)}^{12})^2}}. \quad (42)$$

Substituting in Eq. (29) one obtains

$$\begin{aligned} \tilde{\Sigma}_{a(n)}^{12} &= \Delta_a^{\text{BCS}} - \sum_{b,m} V_{\text{ind}}[a(n)b(m)] N_{b(m)} \\ &\quad \times \frac{\tilde{\Sigma}_{b(m)}^{12}}{2\sqrt{(\epsilon_b - \epsilon_F + \tilde{\Sigma}_{b(m)}^{\text{even}})^2 + (\tilde{\Sigma}_{b(m)}^{12})^2}}. \end{aligned} \quad (43)$$

The second term in this equation is a generalization of the usual BCS gap equation and clearly demonstrates how the action of the different fragments of the original quasiparticles is modulated by their quasiparticle strength $N_{b(m)}$. The equation, however, is of little practical use as it stands because it involves the energy dependent interaction V_{ind} which contains a ‘‘dangerous’’ denominator [cf. Eq. (30)]. The formula is further discussed in Sec. III A4, and we present a similar expression in Sec. II B [cf. Eqs. (53) and (54)].

The approach presented so far (and in Ref. [30]) neglects the $1qp$ -exchange interaction between the complex $1qp \otimes 1ph$ states (see Figs. 6.10(c) and 6.10(d) in Ref. [16]). In fact, the associated matrix elements are set to 0 in the matrix (1). The ignored processes would account for violation of the Pauli principle arising from the microscopic structure of the QRPA phonons, which may imply double occupation of the quasiparticle state in the complex $1qp \otimes 1ph$ state. These violations are small for the calculation reported in this paper.

Those processes account also for vertex renormalization terms in the self-energy, which are not taken into account in the rainbow series we have considered. While in condensed matter they are usually neglected based on the Migdal theorem, in nuclear physics they are usually considered to be of minor importance because their contribution to the self-energy implies a recoupling of angular momenta that owing to the incoherent contributions from all possible intermediate states is expected to lead to a rather strong cancellation [36,37]. As we have mentioned discussing approximation (ii) above, we assume that they are implicitly included in our effective $\langle a; \lambda | H_C | b \rangle$ coupling matrix elements, computed making use of phenomenological phonons and single-particle levels.

Although within NFT tadpole diagrams should be included [17], we neglect the energy-independent contributions associated with them (cf. Fig. 4), which take into account the effect of zero-point fluctuations on the quasiparticle energy [38]. This kind of diagram modifies the nuclear density (cf. Fig. 5) and plays an important role in the calculation of nuclear radii [39–41], representing the leading correction beyond mean field for closed-shell nuclei, and producing sizable isotopic effects [42]. However, they lead to relatively small changes in the mean-field potential. The shifts of the single-particle energies for $A = 120$ can be estimated to be of the order of 150 keV [43], and, being of static nature, we assume that they are effectively taken into account in the mean field. The tadpole diagrams can also influence the abnormal density and the calculation of the bare pairing gap [44], but no

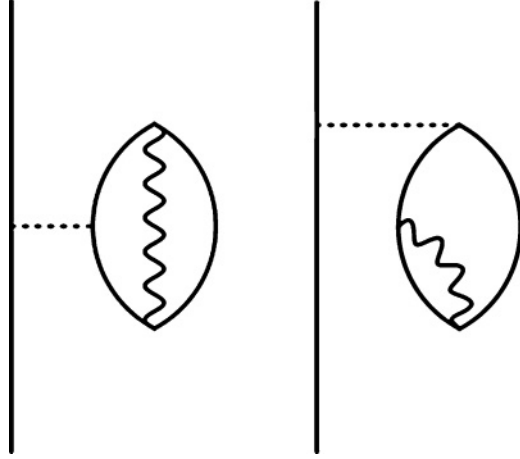


FIG. 4. Lowest-order diagrams representing the renormalization of the quasiparticle self-energy by zero-point fluctuations.

calculations have been performed for superfluid nuclei. We have estimated that the effect of diagrams (a) and (b) displayed in Fig. 5 changes the pairing field by about 5%, evaluating the expression

$$\delta\kappa(r) = \sum_{ab\lambda} (2\lambda + 1) Y_{ab\lambda}^2 \kappa_a(r) / (2j_a + 1), \quad (44)$$

for the change introduced in the abnormal density κ , where $Y_{ab\lambda}$ denotes a backward amplitude calculated in QRPA. Diagrams (c) and (d) give, in the normal case, a contribution to the renormalization of the mean square radius which is about three times larger than the one produced by (a) and (b) [39]. This can be considered as an upper limit because the strong r^{-2} dependence tends to enhance their relative importance.

Thus, we estimate that total effect of tadpole diagrams on the pairing field should be less than 20%, that is, less than 200 keV, which is a number rather consistent with that estimated above for the normal single-particle energy.

Finally, it is of note that the formalism presented in this section is similar to the one adopted by Avdeenkov and Kamerdzhiev [45,46]. However, it is difficult to make a precise comparison of their results with ours, because they have followed a different approach, trying to extract “bare” single-particle levels and pairing gaps from the experimental levels, instead of renormalizing the levels obtained from an effective mean field.

B. The one-step diagonalization scheme

In the previous section we have outlined the two-step diagonalization scheme in the calculation of the pairing

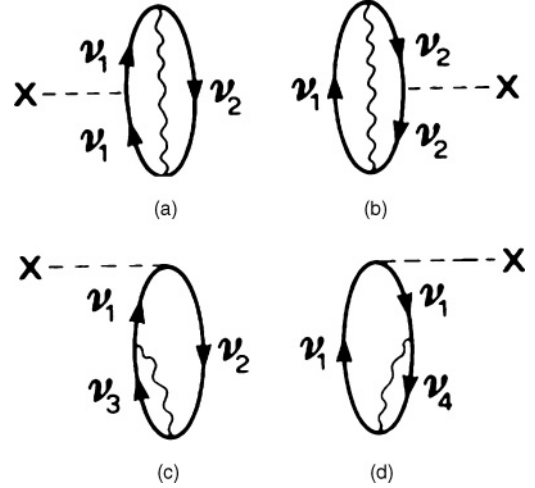


FIG. 5. Lowest-order diagrams representing the renormalization of the density operator (represented by the cross) by zero-point fluctuations in closed-shell nuclei.

properties of superfluid nuclei. That is, we have started from a HF + BCS calculation which accounts for the bare pairing interaction and we have then added medium renormalization effects by diagonalizing the matrix in Eq. (1). However, one could also adopt a different scheme (which we call the one-step diagonalization scheme) in which one starts from the HF solution and then one includes simultaneously both renormalization effects and the bare pairing interaction through the iterative procedure. This approach is particularly appropriate when the phonon-induced pairing provides the leading contribution to pairing correlations and is certainly needed when the bare interaction alone is not able to produce a superfluid solution. This is the case, for instance, in calculations of the structure of halo nuclei [47,48]. However, the two-step diagonalization is more natural, in the framework of general schemes based on the corrections to mean-field properties.

In the Appendix we apply the one-step diagonalization scheme to the calculation of pairing properties in ^{120}Sn , which is a well-bound, superfluid nucleus. In this case we expect that the two schemes should give similar results concerning physically relevant quantities, namely, quasiparticle energies, spectroscopic factors, and pairing gaps.

The one-step diagonalization is performed by introducing the bare pairing field $\Sigma^{12\text{bare}}$ associated with the bare interaction in Eq.(1) by writing

$$\begin{pmatrix} E_a & V(ab\lambda\nu) & V(ac\lambda\nu) & W(ab\lambda\nu) & W(ac\lambda\nu) & \mp\Sigma_a^{12\text{bare}} \\ V(ab\lambda\nu) & \hbar\omega_{\lambda\nu} + E_b & 0 & 0 & 0 & W(ab\lambda\nu) \\ V(ac\lambda\nu) & 0 & \hbar\omega_{\lambda\nu} + E_c & 0 & 0 & W(ac\lambda\nu) \\ W(ab\lambda\nu) & 0 & 0 & -\hbar\omega_{\lambda\nu} - E_b & 0 & -V(ab\lambda\nu) \\ W(ac\lambda\nu) & 0 & 0 & 0 & -\hbar\omega_{\lambda\nu} - E_c & -V(ac\lambda\nu) \\ \mp\Sigma_a^{12\text{bare}} & W(ab\lambda\nu) & W(ac\lambda\nu) & -V(ab\lambda\nu) & -V(ac\lambda\nu) & -E_a \end{pmatrix} \begin{pmatrix} x_{a(n)} \\ C_{a(n),b,\lambda\nu} \\ C_{a(n),c,\lambda\nu} \\ -D_{a(n),b,\lambda\nu} \\ -D_{a(n),c,\lambda\nu} \\ -y_{a(n)} \end{pmatrix} = \tilde{E}_{a(n)} \begin{pmatrix} x_{a(n)} \\ C_{a(n),b,\lambda\nu} \\ C_{a(n),c,\lambda\nu} \\ -D_{a(n),b,\lambda\nu} \\ -D_{a(n),c,\lambda\nu} \\ -y_{a(n)} \end{pmatrix}, \quad (45)$$

where now the unperturbed “quasiparticle” energy E_a contains no contribution from pairing and is simply equal to the difference between the HF single-particle energy and the Fermi energy,

$$E_a = |\epsilon_a - \epsilon_F|,$$

where $\Sigma^{12\text{bare}}$ obeys the equation

$$\Sigma_a^{12\text{bare}} = - \sum_{b,m} V_{\text{bare}}[ab] \frac{(2j_b + 1)}{2} \tilde{u}_{b(m)} \tilde{v}_{b(m)}, \quad (46)$$

and the $-$ ($+$) sign is to be used for particle (hole) states, that is, $\epsilon_a > \epsilon_F$ ($\epsilon_a < \epsilon_F$).

The amplitudes $\tilde{u}_{a(n)}$, $\tilde{v}_{a(n)}$ are given by Eq. (4), taking into account the fact that the initial u_a and v_a factors to be inserted in the iterative solution of Eq. (1) are now equal to 1 or 0, depending on whether the level is above or below the Fermi energy:

$$\tilde{u}_{a(n)} = x_{a(n)}, \quad \tilde{v}_{a(n)} = y_{a(n)}, \quad (47)$$

and

$$\tilde{u}_{a(n)} = -y_{a(n)}, \quad \tilde{v}_{a(n)} = x_{a(n)}, \quad (48)$$

respectively, in the case of a particle and a hole state.

Note that, putting the V – W matrix elements to zero, Eq. (46) reduces to the standard BCS equation for the pairing gap. The solution must be obtained through a self-consistent iterative procedure which in the general case involves simultaneously the bare interaction and the particle-vibration coupling vertices V and W . In general, this is not equivalent to the two-step diagonalization scheme, in which one considers first only $\Sigma^{12\text{bare}}$ (which is exactly equivalent to solve the bare BCS problem) and then takes into account the matrix elements V 's and W 's. Nevertheless, the two schemes lead to similar results, as long as the first diagonalization leads to a finite value of the order parameter, the pairing gap (cf. Appendix, Fig. 26 and related discussion).

As in the two-step scheme, one can use the 2×2 energy-dependent BCS-like matrix to solve the problem. The only difference with respect to Eq. (35) is that now the renormalized pairing gap must include a term $\Sigma^{12\text{bare}}$ representing the contribution of the bare pairing interaction:

$$\tilde{\Delta}_{a(n)} = Z_{a(n)} \left(\Sigma_a^{12\text{bare}} + \tilde{\Sigma}_{a(n)}^{12,\text{pho}} \right) = \tilde{\Delta}_{a(n)}^{\text{bare}} + \tilde{\Delta}_{a(n)}^{\text{pho}}. \quad (49)$$

This expression can be rewritten in the more appealing way,

$$\tilde{\Delta}_{a(n)} = -Z_{a(n)} \sum_{b,m} \frac{(2j_b + 1)}{2} V_{\text{eff}}[a(n)b(m)] \tilde{u}_{b(m)} \tilde{v}_{b(m)}, \quad (50)$$

where one has introduced the effective interaction V_{eff} , which is the sum of the bare and phonon-induced interactions:

$$V_{\text{eff}}[a(n)b(m)] = V_{\text{bare}}[ab] + V_{\text{ind}}[a(n)b(m)]. \quad (51)$$

Furthermore, one can obtain a very closed form for the gap equation by eliminating the amplitudes u and v using

Eq. (35):

$$\begin{aligned} \tilde{u}_{a(n)} \tilde{v}_{a(n)} &= N_{a(n)} \frac{\tilde{\Delta}_{a(n)}}{2\tilde{E}_{a(n)}} \\ &= N_{a(n)} \frac{Z_{a(n)} \tilde{\Sigma}_{a(n)}^{12}}{2\sqrt{Z_{a(n)}^2 (\epsilon_a - \epsilon_F + \tilde{\Sigma}_{a(n)}^{\text{even}})^2 + (Z_{a(m)} \tilde{\Sigma}_{a(n)}^{12})^2}}, \end{aligned} \quad (52)$$

leading to

$$\begin{aligned} \tilde{\Delta}_{a(n)} &= Z_{a(n)} \tilde{\Sigma}_{a(n)}^{12} \\ &= -Z_{a(n)} \sum_{b,m} \frac{(2j_b + 1)}{2} V_{\text{eff}}[a(n)b(m)] N_{b(m)} \\ &\quad \times \frac{\tilde{\Sigma}_{b(m)}^{12}}{2\sqrt{(\epsilon_b - \epsilon_F + \tilde{\Sigma}_{b(m)}^{\text{even}})^2 + (\tilde{\Sigma}_{b(m)}^{12})^2}}. \end{aligned} \quad (53)$$

We note that for levels near to the Fermi energy the Z factor is very close to the quasiparticle strength N . A more compact expression, bearing a direct resemblance to the standard BCS gap equation, may be obtained by reintroducing the Z function both in the numerator and in the denominator:

$$\tilde{\Delta}_{a(n)} = -Z_{a(n)} \sum_{b,m} V_{\text{eff}}[a(n)b(m)] N_{b(m)} \frac{\tilde{\Delta}_{b(m)}}{2\tilde{E}_{b(m)}}. \quad (54)$$

This equation is a consequence of the Nambu-Gor'kov energy-dependent problem and can be used as a useful starting point for approximating gap equations (see Sec. III A4). In particular, restricting the sum to the main peak $m = 1$ and neglecting the difference between N and Z , Eq. (54) formally reduces to an approximate gap equation previously presented in the case of uniform matter ([49] [cf. Eq. (12)], [50]).

III. RESULTS

In the following we present the solution of the Nambu-Gor'kov equations of NFT renormalization processes for ^{120}Sn in various approximations. In all cases, we limit our attention to the five neutron levels belonging to the shell around the Fermi energy (namely, the $1g_{7/2}$, the $2d_{5/2}$, the $3s_{1/2}$, the $2d_{3/2}$, and the $1h_{11/2}$ orbitals). Most of the calculations are performed in the two-step diagonalization scheme, making use of the Argonne nucleon-nucleon interaction as the bare pairing force in the 1S_0 channel, which gives by far the dominant contribution to $T = 1$, $J = 0$ pairing [51]. In the Appendix we also show a few results obtained with the V_{lowk} potential.

In general, we iterate the renormalization process. This requires looking for a self-consistent solution, either by successive diagonalizations of the matrix (1) or (45) or by looking for the solutions of the equivalent energy-dependent 2×2 problem (19). Nearly all of the results presented in this work have been obtained from the first diagonalization procedure. However, we have verified in several instances the numerical agreement between the two methods of solution. To control the iteration process, one must introduce a cutoff procedure, or perform some averaging, to avoid the exponential increase of the number of solutions, retaining at the same time the

essential information [52,53]. We make use of two simple numerical procedures. A cutoff procedure can be adopted when one solves the energy-dependent problem. In this case one can limit the number of solutions kept at each iteration by selecting only those fragments carrying a quasiparticle strength larger than a given cutoff N_{cut} . An extreme case is represented by the so-called one-quasiparticle approximation, in which one keeps only the most important pole for each orbital. We instead make use of an averaging procedure when we solve the energy-independent problem diagonalizing the matrices (1) or (45). In this case, we define a number N_{zones} of energy zones. The zones are generally not of the same size, but are chosen so as to reflect the main features of the quasiparticle strength function. After each iteration we collect all the strength obtained within a given energy zone into a single fragment, placed at the calculated average energy position. In this way, the number of solutions associated with a given orbital a is kept fixed to $N_{\text{dim}} = 2 \times [N_{\text{pho}} \times N_{\text{sps}} \times N_{\text{zones}} + 1]$, where N_{pho} is the number of RPA solutions retained in the diagonalization and N_{sps} is the number of single-particle levels coupled to a .

We compute the basic vertices h [cf. Eq. (16)] controlling the quasiparticle-vibration coupling by first performing a QRPA calculation with the separable force (11) for the multipolarities and parities $\lambda^\pi = 2^+, 3^-, 4^+$, and 5^- . In each case, the coupling constant is determined so as to reproduce the experimental value of the ratio $B(E\lambda)/\hbar\omega_{\lambda,1}$ [cf. the discussion about the approximation (ii) in Sec. II above]. Experimental data are taken from Ref. [54]. The quasiparticle states used in the QRPA calculation are obtained from a BCS calculation with a monopole pairing interaction $-G_0 P^\dagger P$ based on the levels of a Woods-Saxon potential parametrized as in Ref. [33], Eq. (2-182). The pairing coupling constant G_0 is adjusted so as to reproduce the value $\Delta_{\text{exp}} \approx 1.4$ MeV derived from the experimental odd-even mass difference.

Concerning the QRPA spectrum, we adopt an averaging procedure similar to that adopted for the quasiparticle strength. We include explicitly the strong collective low-lying vibrational states and we collect the remaining strength in a small number of peaks, reflecting the gross structure of the response for each multipolarity [9]. We have verified that the results are not sensitive to the details of the distribution of high-lying phonons. The properties of the low-lying phonons employed in the calculations are listed in Table I, where they are compared with the available experimental data. We remark that the values of χ_λ [cf. Eq. (11)] are close to 0.9, reflecting the rather good accuracy of the collective model.

A. Calculations with bare pairing potentials

In this section, we discuss solutions of the Nambu-Gor'kov equations making use of bare nucleon-nucleon potentials as pairing interactions. As we have remarked above, we adopt the two-step diagonalization scheme. The practical difficulty using a one-step diagonalization in this case is that the basis needed to account for the realistic bare interactions must span a broad energy interval (about 1 GeV in the case of the Argonne v_{14} interaction and about 200 MeV in the case of $V_{\text{low}k}$). This implies a large numerical effort to handle Eq. (45), in particular

TABLE I. In the first columns we list the experimental energies $\hbar\omega_{\lambda,1}$ in (MeV), deformation parameters $\beta_{\lambda,1}$, and polarizabilities $\beta_{\lambda,1}^2/\hbar\omega_{\lambda,1}$ of the low-lying states associated with the 2^+ , 3^- , 4^+ , and 5^- multipolarities. They are compared with the corresponding quantities calculated in QRPA, making use of the effective deformation parameter $\beta_{\lambda,1}^{\text{eff}} = \chi_\lambda \beta_{\lambda,1}$. In the last column we give the values of χ_λ . In the case of 4^+ , the experimental low-lying strength is fragmented in four peaks lying between 2.2 and 3.8 MeV; the numbers in the table refer to an average weighted with the transition strength of each peak.

| λ^π | Exp. | | | Theory | | | |
|---------------|---------------------------|---------------------|---|---------------------------|----------------------------------|--|----------------|
| | $\hbar\omega_{\lambda,1}$ | $\beta_{\lambda,1}$ | $\beta_{\lambda,1}^2/\hbar\omega_{\lambda,1}$ | $\hbar\omega_{\lambda,1}$ | $\beta_{\lambda,1}^{\text{eff}}$ | $(\beta_{\lambda,1}^{\text{eff}})^2/\hbar\omega_{\lambda,1}$ | χ_λ |
| 2^+ | 1.17 | 0.13 | 0.014 | 1.20 | 0.13 | 0.013 | 0.86 |
| 3^- | 2.40 | 0.16 | 0.011 | 2.71 | 0.16 | 0.010 | 0.95 |
| 4^+ | 3.10 | 0.11 | 0.004 | 2.33 | 0.10 | 0.004 | 0.91 |
| 5^- | 2.27 | 0.08 | 0.003 | 2.48 | 0.09 | 0.003 | 0.91 |

because the matrix associated with a given angular momentum must include states with different numbers of nodes. We further consider the relation between the one- and two-step diagonalization schemes presented in Sec. II, making use of a simplified bare interaction.

1. Bare pairing gap

The first step in our calculation is represented by the solution of the HF + BCS equation with the bare force in the pairing channel; we do not consider the influence of pairing on the mean field.

It is of note that the calculation with the bare force is, in fact, an extended BCS calculation. This is because for a hard-core interaction it is essential to consider the coupling between pairs of levels with different numbers of nodes to take properly into account the coupling between bound and continuum levels [55,56]. We include states up to 1 GeV. As a consequence, for given quantum numbers $\{lj\}$ one obtains a set of quasiparticle energies $\{E_k\}$; to each quasiparticle is associated an array of quasiparticle amplitudes u_{nk} and v_{nk} , which are the components of the quasiparticle states over the HF basis states ϕ_{nlj} . Going to the canonical basis, where the density matrix takes a diagonal form [57], we look for the state having the largest value of the abnormal density, $u_{\text{max}}v_{\text{max}}$. As a rule, for a stable nucleus such as ^{120}Sn , this canonical state is dominated by the quasiparticle state having the lowest value of the quasiparticle energy, E_{min} . We then approximate the extended BCS calculation associating the value of v_{max} and E_{min} , treating them as proper BCS quantities; in particular, we derive an associated pairing gap as $\Delta^{\text{BCS}} = 2u_{\text{max}}v_{\text{max}}E_{\text{min}}$, which is very close to the diagonal value of the gap in the original basis. The value of u_{max} , v_{max} , E_{min} are then employed as input values for the solution of the Nambu Gor'kov equations in the two-step diagonalization scheme described in Sec. II A [cf. Eqs. (1) and (4), where they are denoted u_a , v_a and E_a]. This approximation leads to a substantial simplification of our numerical scheme.

For nuclei close to the line of stability, where the canonical states have significant weight on continuum state and the basic vertices associated with the coupling term H_C (see, e.g., Ref. [18]) can easily connect bound and continuum states, this approximation would not be justified and one should rather consider different numerical schemes, for example, based on the continuum Green's function.

The mean field is taken from a HF calculation with the SLy4 interaction [58]. This interaction gives a good reproduction of the bulk properties of nuclei; moreover, the resulting level density close to the Fermi energy (associated with an effective mass $m_k \approx 0.7m$), once increased by renormalization effects, is in reasonable agreement with the experimental one (the associated effective mass increasing to $m^* = m_k m_\omega \approx m$). The energies of the five single-particle levels lying closest to the Fermi energies are shown in the Appendix (cf. Fig. 16). The detailed features of our calculations are, of course, influenced by the specific properties of the mean field and in particular by its effective mass. To have some insight about the dependence on the adopted mean field, in the Appendix we provide results obtained making use of two different Skyrme interactions, having effective masses smaller and larger than the SLy4 interaction. One should distinguish two different effects that influence the pairing gap Δ^{BCS} calculated with the bare pairing interaction: On the one hand, the pairing gap is sensitive to the detailed position of the levels close to the Fermi energy, which could be influenced by static contributions not considered here, as those produced from tensor correlations [59,60] and from tadpole diagrams [44] (for the latter, cf. the comments at the end of Sec. II A); on the other hand, the pairing gap is also sensitive to the momentum dependence of m_k for large momenta.

In a previous work [11] we presented a solution of the HFB equations using the Argonne v_{14} equation in the pairing channel, which led to a pairing gap of the order of 700 keV. There we used a modified SLy4 mean field, reducing the

spin-orbit coupling strength by about 15% (furthermore, we included in the Hamiltonian the terms proportional to the square of the spin density, which are instead not considered in the following, and used a slightly larger particle vibration coupling strength). This was done to improve the agreement of the results obtained after renormalization with the experimental spectrum and pairing gap. Here we prefer to take the HF field obtained with the original SLy4 interaction. This is associated with a larger level density around the Fermi energy. As a consequence, the obtained pairing gap Δ^{BCS} , shown in Fig. 6(a) (full dots), is larger, being equal to about 1.1 MeV. Similar calculations have been performed with the V_{lowk} potential using the same mean field [61]. In that case, the result depends on the cutoff Λ adopted to obtain V_{lowk} : For values of Λ smaller than about 4 fm^{-1} , the gap is close to 1.4 MeV, (cf. Fig. 22), while for increasing values of Λ the V_{lowk} potential reduces to the Argonne potential and one obtains the result shown in Fig. 6(a). We notice that our numerical results with the Argonne potential are in very good agreement with those reported in Ref. [61] for very large values of Λ . The reason for the difference between the results obtained with the Argonne and V_{lowk} interaction has been discussed in detail [61,62]: Using the Argonne potential implies using the Skyrme effective mass m_k (equal to about $0.7m$ inside the nucleus) up to very high momenta, while the renormalization process leading to V_{lowk} implies that m_k goes to the free mass for momenta larger than the cutoff Λ . The lower value of m_k at high momenta leads to a smaller level density and to a reduction of about 300 keV in the value of the gap with the Argonne interaction with respect to the values obtained with V_{lowk} for cutoffs Λ up to about 4 fm^{-1} . An analogous difference shows up in calculation of the gap in uniform matter. While the lack of momentum dependence of the effective mass associated with Skyrme interactions is certainly unrealistic, the proper momentum dependence is still to be established. On the other hand, the density dependence of m_k associated with the SLy4

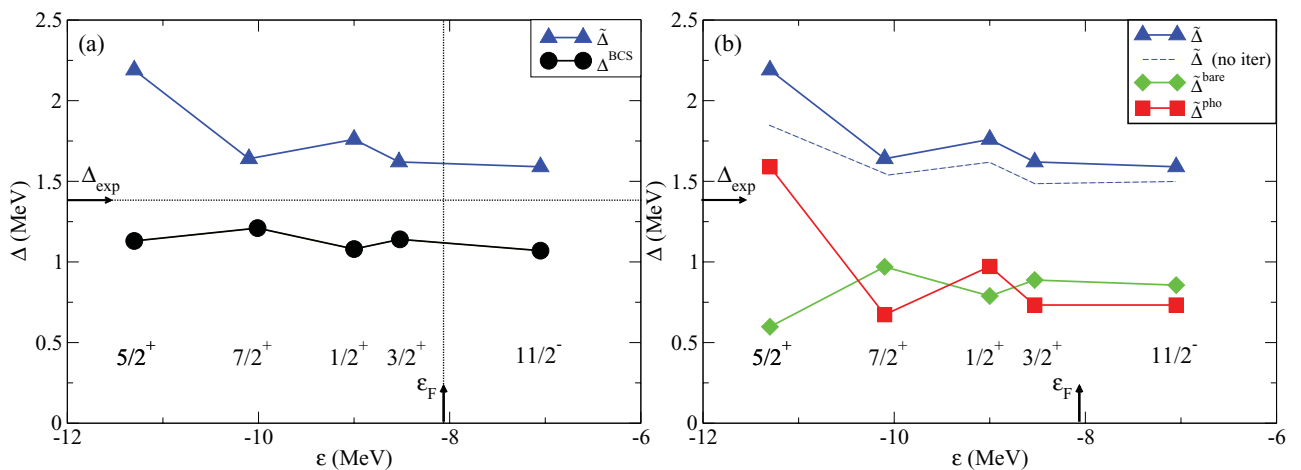


FIG. 6. (Color online) (a) The state-dependent neutron pairing gap Δ^{BCS} calculated in BCS with the bare v_{14} interaction is shown as a function of the SLy4 HF single-particle energy of the five valence orbitals (cf. Fig. 16) and is compared to the renormalized gap $\tilde{\Delta}$ [cf. Eq. (38)] obtained solving the Nambu-Gor'kov equations by iteration. The values of the Fermi energy ϵ_F and of the gap obtained from the experimental odd-even mass difference Δ_{exp} are also indicated. (b) We show the decomposition of the renormalized gap $\tilde{\Delta}$ into the bare and phonon contributions $\tilde{\Delta}^{\text{bare}}$ and $\tilde{\Delta}^{\text{pho}}$. Also shown is the gap obtained at the first iteration.

interaction in nuclear matter is not far from that resulting at the Fermi energy from calculations based on Brückner theory [62]. Furthermore, a precise determination of the value of the bare gap within the V_{lowk} scheme requires the consideration of the effects of the three-body force, which is expected to provide a repulsive contribution [63]. A calculation of three-body effects within the V_{lowk} renormalization scheme [64,65] leads in fact to a reduction of the gap, down to values close to those obtained with the Argonne interaction shown in Fig. 6(a). An average value of the bare gap close to 1 MeV was also derived in the analysis of Refs. [45,46].

We have brought circumstantial evidence which testifies to the fact that a pairing gap $\Delta^{BCS} \approx 1.1$ MeV for the levels around the Fermi energy obtained using the v_{14} potential as bare pairing interaction and the effective mass associated with SLy4 represents a reasonable starting point, being well aware that the determination of the mean field and of the associated effective mass is one of the most important issues that remains to be fully clarified, for a quantitative and microscopic calculation of the gap in finite nuclei. In the Appendix we investigate the dependence of the results on the adopted mean field, and we provide some results obtained adopting V_{lowk} as bare pairing interaction.

2. Solution of the Nambu-Gor'kov equations

The state-dependent pairing gap obtained from the solution of the Nambu-Gor'kov equations is compared to the bare gap in Fig. 6(a). Renormalization effects lead to a total gap $\tilde{\Delta}$ about 600 keV larger than Δ^{BCS} . Most of the effect is obtained already with the first diagonalization of the Nambu-Gor'kov matrix. The self-consistent iteration process leads to a further increase of the gap by about 10%. We recall that one can distinguish two contributions to the renormalized gap $\tilde{\Delta} = Z[\Delta^{BCS} + \tilde{\Sigma}^{12,pho}] = \tilde{\Delta}^{bare} + \tilde{\Delta}^{pho}$, associated with the bare and with the phonon-induced interaction [cf. Eq. (38)]. They are shown in Fig. 6(b) and turn out to be of similar magnitude. This confirms that the phonon-induced pairing interaction is as important as the bare interaction in determining pairing properties of heavy nuclei. Notice that a proper comparison between the role of these two sources of pairing can only be made analyzing their contribution to the final physical result and not just by comparing the BCS and complete pairing gaps. In fact, processes beyond mean field act in a complex way, not only giving rise to the induced pairing interaction, but also changing the effect of the bare interaction through the Z factors. The values of Z for the five orbitals are shown in Fig. 7 where it can be seen that they are close to 0.7, bringing the bare contribution $\Delta^{BCS} \approx 1.1$ MeV down to $\tilde{\Delta}^{bare} \approx 0.8$ MeV, which is about one half of the total renormalized gap. The other half is provided by the pairing induced interaction. The values of Z are similar to the values of the quasiparticle strength $N = U^2 + V^2$, except for the orbital $d_{5/2}$. It is seen that these values of N provide an overall account of the quasiparticle strength measured in one-nucleon transfer reactions, shown by stars in Fig. 7 (cf. also below Figs. 8–10 with the related discussion), although one has to consider that the experimental values are affected by a large error, estimated to be about 30%.

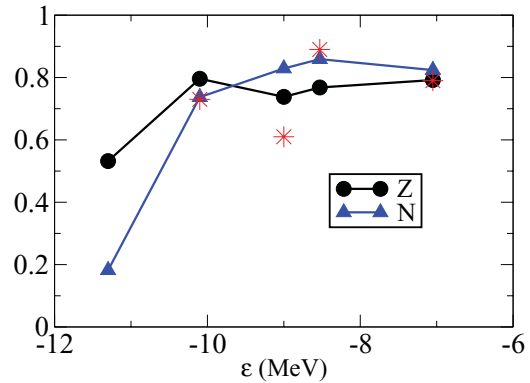


FIG. 7. (Color online) Comparison of the N and Z factors associated with the lowest quasiparticle peaks in the Nambu-Gor'kov calculation. Also shown by stars are the values of the experimental quasiparticle strength [66], except for the $d_{5/2}$ orbital, which shows a pronounced fragmentation (cf. text).

The renormalized pairing gap exceeds the experimental value obtained from the odd-even mass difference by about 300 keV, the value of Δ_{exp} lying in between Δ^{BCS} and $\tilde{\Delta}$. It is of note that the estimate of Δ_{exp} varies by about ± 100 keV depending on which odd-even mass formula is used [67,68] (the five-point formula $\Delta^{(5)}$ yielding a value of 1.39 MeV) and that a more consistent comparison would imply a theoretical calculation of the binding energies. Such a precise comparison of the gaps is probably not very significant at the present stage, given the uncertainties that affect both the BCS calculation, such as the dependence on the adopted HF mean field and the effect of three-body forces mentioned above, and the renormalization process, in particular the exchange of spin modes, not included in this calculation (see the discussion in Secs. III A3 and IV). Nonetheless, the necessity of going beyond mean field is very clear considering other physical quantities, in particular the energy spectrum of neighboring odd nuclei together with the associated strength functions and spectroscopic factors. This can be seen in Fig. 8 where we compare the features of the quasiparticle spectrum obtained at the different steps of the calculation. In the first column (HF), we report the absolute value of the difference $|\epsilon_a - \epsilon_F|$ obtained in the HF calculation with the SLy4 force, referred to the value of this difference for the level $d_{3/2}$, which lies closest to the Fermi energy $\epsilon_F = -8.05$ MeV (cf. Fig. 16). In the second column (v_{14}), we give the values of the quasiparticle energies obtained in the HF + BCS calculation with the Argonne force, referred to the lowest quasiparticle. In the third column (NFT0) we show the spectrum obtained taking into account processes beyond mean field calculated with the Nambu-Gor'kov equations without iterating, while in the fourth (NFT) we show the self-consistent solution: In these cases we show the energy of the lowest fragment for each quantum number (this is also the one collecting the largest quasiparticle strength, except for the $d_{5/2}$ orbital, which is very fragmented and whose case is discussed below). Finally, in the fifth and sixth columns we give the position of the lowest peaks measured in ^{119}Sn and ^{121}Sn . The main discrepancy of the renormalized spectrum concerns the $7/2^+$ state. This is probably related to the initial position of the $g_{7/2}$ orbital in the HF spectrum calculated with

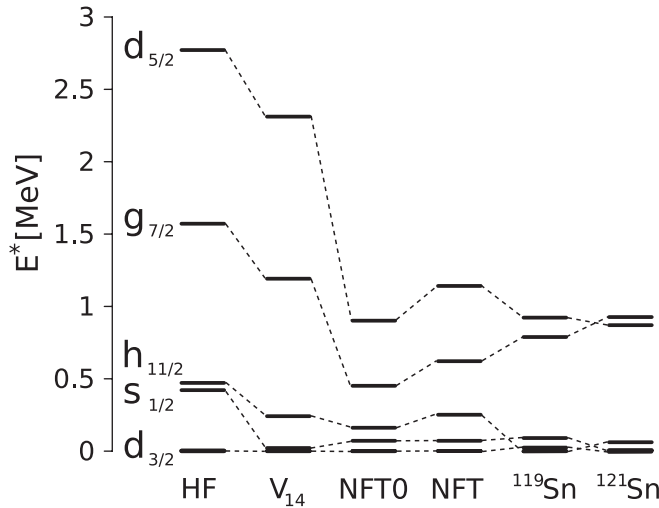


FIG. 8. The theoretical quasiparticle spectra obtained at the various steps of the calculation are compared to the experimental data. See the text for more explanation.

the SLy4 interaction, which lies too close to the Fermi energy (cf. Fig. 16). The experimental energies of the lowest three states are very close to each other, being separated by less than 100 keV, and are well separated from the other two levels. This gross structure is already present in the HF result, which, however, greatly underestimates the density of levels. This remains the case including pairing correlations at the BCS level (see second column), which lead to a limited improvement. Renormalizing effects owing to the processes shown in Fig. 1 lead to a denser spectrum, considerably improving the agreement with experiment, although one should not expect a detailed agreement in the order of the three lowest levels. The main effect is already obtained with a single diagonalization (NFTO), but the self-consistent treatment (NFT) leads to an appreciable rearrangement of the spectrum, somewhat reducing the initial compression of the levels, slightly improving the agreement with experiment. The increase of level density can be expressed as an increase of the neutron effective mass from $m^* \approx 0.7m$ to $m^* \approx m$. One could argue that a mean-field BCS calculation in a potential with $m^* = 1$ would lead to agreement with experiment in a simpler and more direct way. However, such a calculation (still performed with the bare interaction) would greatly overestimate the gap [69]. Thus, the simultaneous consideration of gap and low-energy spectra clearly favors a description that includes renormalization effects on both quantities.

The most specific fingerprint of the renormalization processes is represented by the fragmentation of the quasiparticle strength. Experimentally, the effects of such a fragmentation lead to a breaking of the observed quasiparticle strength into several peaks and consequently to a reduction of the strength observed in the main peaks, as compared to the full strength expected in mean-field calculations. In the present case, strength functions measured in one-neutron transfer experiments involving ^{119}Sn or ^{121}Sn [66,70,71] show a strong, isolated peak for the quantum numbers $J^\pi = 1/2^+, 3/2^+, 7/2^+, 11/2^-$. The case of $11/2^-$ is shown in Fig. 9, where we compare the theoretical values of \tilde{v}^2 (\tilde{u}^2)

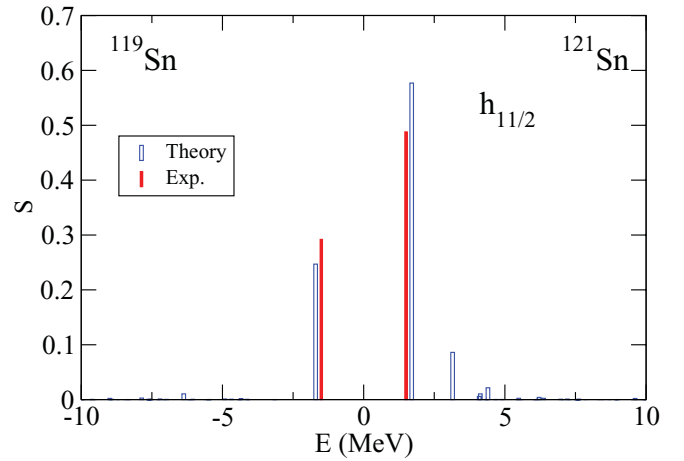


FIG. 9. (Color online) The theoretical strength function calculated for the $h_{11/2}$ orbital is compared to the spectroscopic factors associated with experimental levels detected in one-neutron transfer reactions.

with the observed peak in ^{119}Sn (^{121}Sn). Here, and in similar figures (such as Fig. 10), to compare the experimental to the theoretical strength functions, we have added the energy of the lowest calculated quasiparticle to the experimental excitation energy in the odd nuclei ^{119}Sn and ^{121}Sn . The summed strength of the two main peaks is equal to 0.79 in experiment and to 0.8 in theory. The remaining theoretical strength is calculated to lie at higher energy in ^{121}Sn . Overall agreement between theory and experiment is found also in the case of the other three levels, as is shown in Fig. 7.

It is interesting to note that the main contribution to the renormalization effects originates from the coupling to the lowest vibrational state of each multipolarity: This demonstrates the key role played by the interweaving of collective and single-particle modes which is at the basis of the NFT treatment of the elementary modes of nuclear excitation.

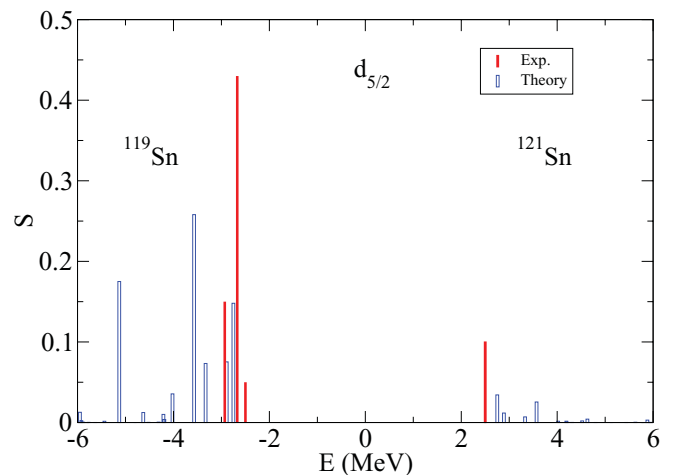


FIG. 10. (Color online) The theoretical strength function calculated for the $d_{5/2}$ orbital is compared to the spectroscopic factors associated with experimental levels detected in one-neutron transfer reactions.

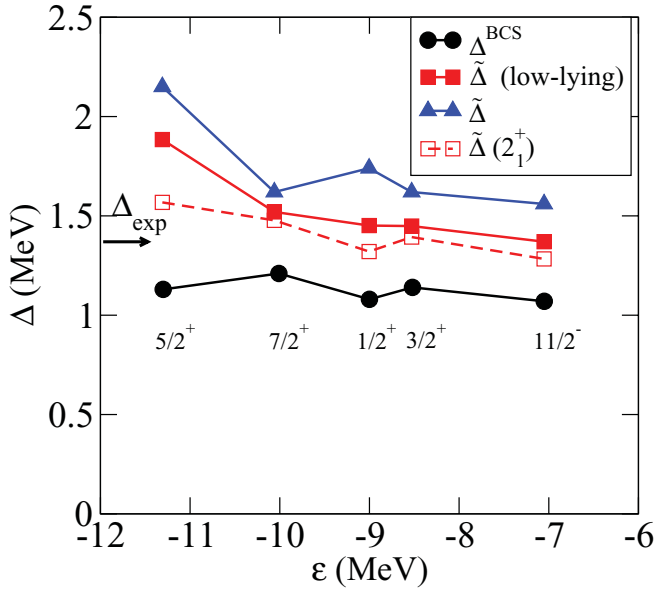


FIG. 11. (Color online) The pairing gaps Δ^{BCS} obtained in the BCS calculation (dots) and $\tilde{\Delta}$ including the renormalization effects (triangles) are compared to those obtained including only the renormalization owing to the coupling to the lowest 2^+ , 3^- , 4^+ , and 5^- QRPA modes (solid squares), or only the lowest 2^+ mode (open squares).

This is clearly seen in Fig. 11, where we compare the full calculations with results obtained including only couplings to the lowest vibrational states. It is seen that the coupling to the 2^+ low-lying mode is the dominant one, providing half of the increase of the gap owing to the renormalization effects. The other low-lying modes provide about one-third of the remaining increase of the gap, while higher energy modes (mainly giant resonances) complete the picture. The strength of the various couplings is reported in Table II, where for each pair of orbitals (a, b) we list the value of the squares of the particle-vibration matrix elements summed over the phonons of a given multipolarity, $\sum_{\nu} h^2(ab\lambda\nu)/(2j_b + 1)$, which enter the numerator of the induced interaction [cf. Eq. (30)]. We observe that although the deformation parameter associated with the lowest 3^- state is the largest one (cf. Table I) its influence is hindered with respect to the 2^+ by its higher energy and by the fact that it acts efficiently only between the $d_{5/2}$ and the $h_{11/2}$ orbitals, which are the only ones having opposite parity and the same spin alignment. We also note that the dominance of the coupling to low-lying vibrational states found in the present calculation makes our approach distinctly different from other approaches based on microscopic calculations of the particle-vibration coupling with zero-range forces, which need an energy cutoff to avoid an ultraviolet divergence in the self-energy [72].

The experimental strength associated with the quantum number $5/2^+$ (cf. Fig. 10) shows a number of low-energy peaks, which exhaust about 63% of the strength. The theoretical distribution is considerably more fragmented than observed in the data; moreover, most of the strength lies about 1 MeV above the experimental findings. This represents an interesting open question. In the calculation, the energy

TABLE II. For each pair (a, b) of the five valence orbitals, we list the value of the sum $\sum_{\nu} h^2(ab\lambda\nu)/(2j_b + 1)$, in MeV^2 . For pairs of orbitals of the same parity, the numbers in the upper (lower) row give the contribution associated with $\lambda = 2^+$ ($\lambda = 4^+$) phonons; for pairs of orbital of different parity, the numbers in the upper (lower) row give the contribution associated with $\lambda = 3^-$ ($\lambda = 5^-$) phonons.

| | $d_{5/2}$ | $g_{7/2}$ | $s_{1/2}$ | $d_{3/2}$ | $h_{11/2}$ |
|------------|----------------|----------------|------------|----------------|----------------|
| $d_{5/2}$ | 0.190 0.088 | 0.016 0.041 | 0.467 0 | 0.071 0.266 | 0.340 0.138 |
| $g_{7/2}$ | 0.016 0.041 | 0.130 0.071 | 0 0.168 | 0.236 0.081 | 0.020 0.043 |
| $s_{1/2}$ | 0.467 0 | 0 0.168 | 0 0 | 0.461 0 | 0 0.389 |
| $d_{3/2}$ | 0.071 0.266 | 0.236 0.081 | 0.461 0 | 0.253 0 | 0 0.092 |
| $h_{11/2}$ | 0.340 0.138 | 0.020 0.043 | 0 0.389 | 0 0.092 | 0.169 0.100 |

of the $d_{5/2}$ quasiparticle is lowered by its strong coupling with $s_{1/2}$ state (through the 2^+ vibrations) and with the $h_{11/2}$ state (through the 3^- vibrations), as can be seen in Table II. These couplings bring the energy of the $d_{5/2}$ state close to the energies of the $s_{1/2} \otimes 2^+$ and $d_{3/2} \otimes 2^+$ configurations. The matrix elements of the induced interaction V_{ind} [cf. Eq. (30)] are listed in Table III. They are calculated using the values of the renormalized quasiparticle energies $\tilde{E}_a(1)$ of the lowest fragment for each orbital. Their values can be compared to the typical value of the matrix elements of the bare interaction, which is about $G_0 = -0.22$ MeV (cf. the Appendix). They are rather well correlated with the matrix elements reported in Table II, with the remarkable exception of $d_{5/2}$: In the latter case, the induced interaction with the orbitals $s_{1/2}$ and $d_{3/2}$ takes large values, associated with the almost degeneracy

TABLE III. Contribution of the phonons of a given multipolarity to the matrix elements of the induced interaction $V_{\text{ind}[a(1)b(1)]}$ [cf. Eq. (30)] between the lowest fragments of the five valence orbitals, in MeV. For pairs of orbitals for the same parity, the numbers in the upper (lower) row give the contribution of the matrix elements involving 2^+ (4^+) phonons; for pairs of orbital of different parity, the numbers in the upper (lower) row give the contribution of the matrix elements involving 3^- (5^-) phonons.

| | $d_{5/2}$ | $g_{7/2}$ | $s_{1/2}$ | $d_{3/2}$ | $h_{11/2}$ |
|------------|------------------|------------------|-------------|------------------|------------------|
| $d_{5/2}$ | -0.223 -0.054 | -0.031 -0.030 | -1.701 0 | -1.230 -0.245 | -0.309 -0.075 |
| $g_{7/2}$ | -0.015 -0.023 | -0.157 -0.045 | 0 -0.117 | -0.513 -0.062 | -0.016 -0.021 |
| $s_{1/2}$ | -0.383 0 | 0 -0.100 | 0 0 | -0.686 0 | 0 -0.177 |
| $d_{3/2}$ | -0.055 -0.139 | -0.219 -0.047 | -0.503 0 | -0.319 0 | 0 -0.041 |
| $h_{11/2}$ | -0.183 -0.051 | -0.012 -0.017 | 0 -0.167 | 0 -0.042 | -0.212 -0.067 |

of the renormalized energy of the $d_{5/2}$ quasiparticle with the configurations $s_{1/2} \otimes 2_1^+$ and $d_{3/2} \otimes 2_1^+$, which leads to the fragmentation of the $d_{5/2}$ strength.

These results may indicate that the unperturbed quasiparticle energy of the $d_{5/2}$ orbital lies too high. In fact, shifting the energy of the single-particle energy by 600 keV toward the Fermi energy, and leaving everything else unchanged, and then solving the BCS and Nambu-Gor'kov equations, one obtains a better agreement with experiment, as is shown below in Sec. IV [cf. Fig. 15(d)]. This is also the case, making use of effective forces different from SLy4 (cf. also the Appendix). This shows that a detailed study of the fragmentation process can give important indications about how to improve the mean field.

3. Effects of spin modes

In the previous sections we have discussed in detail the medium effects associated with the coupling to collective surface vibrations. In this section we make some remarks concerning the coupling to spin modes. Their contribution represents the leading renormalization effect in calculations in uniform neutron matter, where it induces a repulsive contribution on the pairing interaction that wins over the attractive contribution associated with density modes—thanks to the larger multiplicity of spin modes—leading to a quenching of the pairing gap [73–76]. However, one expects that the relative weight of spin modes should be considerably less important in finite nuclei, where there is no equivalent to low-lying surface collective vibrations.

The repulsive character of spin modes, as opposed to density modes, arises from their different transformation properties under time reversal. This is reflected in a sign change in the basic V , W vertices (cf. Eq. (6–207) in Ref. [16]), which become [cf. Eq. (18)]

$$\begin{aligned} V(ab(m)\lambda\nu) &= h_{S=1}(ab\lambda\nu)(u_a\tilde{u}_{b(m)} + v_a\tilde{v}_{b(m)}), \\ W(ab(m)\lambda\nu) &= h_{S=1}(ab\lambda\nu)(-u_a\tilde{v}_{b(m)} + v_a\tilde{u}_{b(m)}). \end{aligned} \quad (55)$$

It can be shown that, as a consequence, the induced pairing interaction V_{ind} changes its sign, leading to a repulsive contribution. On the other hand, the normal self-energies depend on the square of V and W so that their value is increased by the action of spin modes. There is furthermore a change in the expression of the basic vertex h , which is given by

$$\begin{aligned} h_{S=1}(abJ\nu) &= -(-1)^{j_a-j_b}\beta_{J\nu}\langle a|f_J(r)|b\rangle\langle j_b||Y_{\lambda\sigma}||j_a\rangle \\ &\times \left[\frac{1}{(2j_a+1)(2J+1)} \right]^{1/2}, \end{aligned} \quad (56)$$

where $f_J(r)$ is the form factor associated to the $S = 1$ modes transition density.

The contribution of spin modes to pairing correlations in ^{120}Sn was estimated in Ref. [77], based on a QRPA calculation performed with the SkM* interaction. There it was found that, performing a calculation of the pairing gap including only the induced interaction, and using the simplified expression discussed in Sec. III A4 [cf. Eq. (60)], the spin modes decreased the gap arising from the coupling with $S = 0$ modes by about 25%. We have incorporated this effect in our present calculation by introducing a schematic $S = 1$ response function, consisting of a single peak at an energy of about $1\hbar\omega_{\text{osc}}$, in keeping with the fact that, as a rule, there are no low-lying $S = 1$ modes in finite nuclei.

The values obtained for $\tilde{\Delta}$ and for the quasiparticle strength N are shown, respectively, in Figs. 12 and 13. In keeping with their contribution to the normal self-energy, the action of spin modes tends to reduce, although slightly, the value of Z and N . Spin modes also lead to a reduction of $\tilde{\Delta}^{\text{pho}}$ by about 25% (150 keV), which reflects directly the reduction introduced in $\tilde{\Sigma}^{12\text{pho}}$, while the value of $\tilde{\Delta}^{\text{bare}}$ is practically unaffected. Of course, a systematic study of the role that spin, as well as $\sigma \cdot \tau$ and $\tau \cdot \tau$ modes, aside from the density modes considered in the present paper, play in the nuclear spectrum, is needed for a more quantitative assessment of renormalization effects,

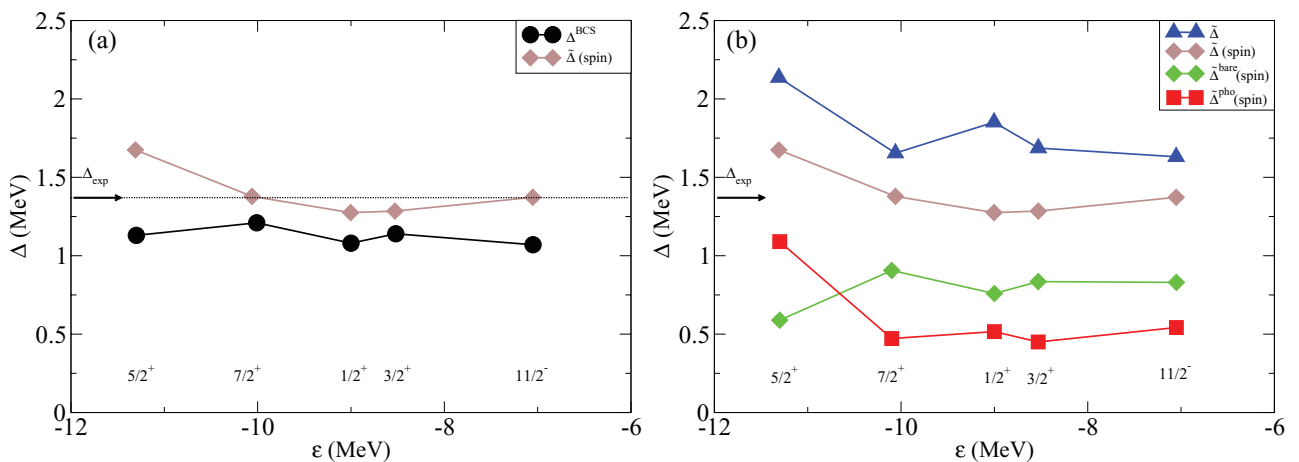


FIG. 12. (Color online) (a) The BCS pairing gap Δ^{BCS} (cf. Fig. 6(a)) is compared with the renormalized pairing gap $\tilde{\Delta}(\text{spin})$ associated with the lowest quasiparticle peaks obtained solving the Nambu-Gor'kov equations including the schematic spin-induced interaction discussed in the text. (b) We show the decomposition of the gap $\tilde{\Delta}(\text{spin})$, shown in (a), into the bare and phonon contributions $\tilde{\Delta}^{\text{bare}}(\text{spin})$ and $\tilde{\Delta}^{\text{pho}}(\text{spin})$. Also shown in the renormalized gap $\tilde{\Delta}$ obtained without the spin-induced interaction (cf. Fig. 6(b)).

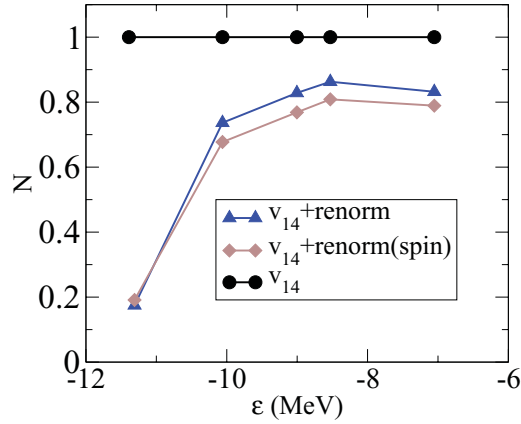


FIG. 13. (Color online) The strength N associated with the main quasiparticle peaks in the bare HF + BCS calculation (dots) and solving the Nambu-Gor'kov equations (triangles) is compared to the result obtained including the schematic spin-induced interaction discussed in the text (diamonds).

considering also $T = 0$ pairing. This will be the main subject of a future presentation.

4. One-quasiparticle approximation and the gap equation

We have seen that the quasiparticle strength function for the states close to the Fermi energy displays a limited amount of fragmentation. If one is only interested in the properties of the main quasiparticle peaks, it may be interesting to solve the Nambu-Gor'kov problem by keeping only the main quasiparticle for each orbital in the iteration process.

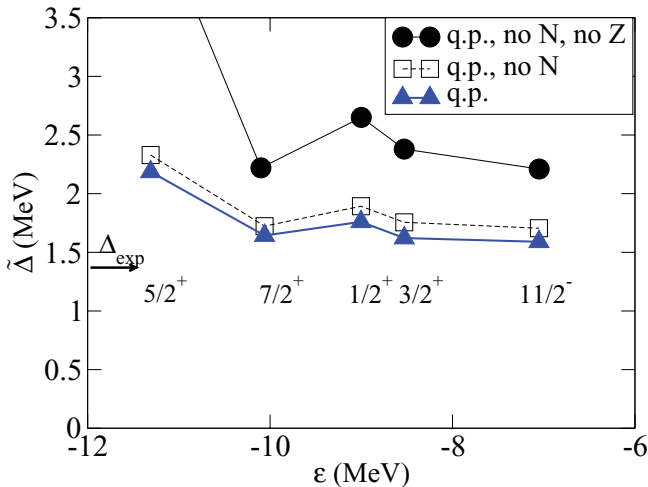


FIG. 14. (Color online) The pairing gaps obtained in the quasiparticle calculation (triangles) are compared to the results obtained neglecting the normalization factors N , and neglecting both N and Z .

We recall the gap equation Eq. (43):

$$\tilde{\Sigma}_{a(n)}^{12} = \Delta_a^{\text{BCS}} - \sum_{b,m} V_{\text{ind}}[a(n)b(m)]N_{b(m)} \times \frac{\tilde{\Sigma}_{b(m)}^{12}}{2\sqrt{(\epsilon_b - \epsilon_F + \tilde{\Sigma}_{b(m)}^{\text{even}})^2 + (\tilde{\Sigma}_{b(m)}^{12})^2}}. \quad (57)$$

The q.p. approximation consists in restricting the sum in Eq. (57) to $m = 1$, obtaining the q.p. self-energy $\tilde{\Sigma}_a^{12\text{q.p.}}$. The resulting values for the q.p. gap $\tilde{\Delta}_a^{\text{q.p.}} = Z_a \tilde{\Sigma}_a^{12\text{q.p.}}$, displayed in Fig. 14, are in excellent agreement with the complete calculation shown in Fig. 6. It is important to note that to get such a good agreement one must include the factors N and Z associated with the quasiparticle peaks. Neglecting them, that is, attributing the full quasiparticle strength to the single peak retained in the calculation, leads to an increase of the gap by about 50%, in keeping with the typical values $Z \approx 0.7$ and $N \approx 0.8$. Neglecting N produces a smaller effect than neglecting Z , because N affects only the induced part of the gap in Eq. (57). The error is especially pronounced for the case of $d_{5/2}$, where the one-quasiparticle approximation selects the lowest peak, which is associated with a small value of N and Z (cf. Fig. 7). From this result, one concludes that the gap receives only very small contributions from the fragments with $m > 1$, which, however, account for more than 20% of the quasiparticle strength. This is mostly attributable to the energy dependence of V_{ind} , which is strongly peaked at the Fermi energy [12].

A gap equation equivalent to Eq. (57) has been obtained in the one-step diagonalization scheme [cf. Eq. (54)]:

$$\tilde{\Delta}_{a(n)} = -Z_{a(n)} \sum_{b,m} V_{\text{eff}}[a(n)b(m)]N_{b(m)} \frac{\tilde{\Delta}_{b(m)}}{2\tilde{E}_{b(m)}}. \quad (58)$$

This expression lends itself to approximations, which are useful to make a connection with previous works about renormalization effects on pairing. The most important feature of these approximations is the use of simplified expressions for the induced interaction V_{ind} [cf. Eq. (30)],

$$V_{\text{ind}}[a(n)b(m)] = \sum_{\lambda,\nu} \frac{2h^2(ab\lambda\nu)}{(2j_b + 1)} \left[\frac{1}{\tilde{E}_{a(n)} - \tilde{E}_{b(m)} - \hbar\omega_{\lambda\nu}} - \frac{1}{\tilde{E}_{a(n)} + \tilde{E}_{b(m)} + \hbar\omega_{\lambda\nu}} \right], \quad (59)$$

based on the Feynman diagram (1c) in Fig. 1 and neglecting fragmentation:

$$V_{\text{ind}}(ab) \approx \sum_{\lambda,\nu} \frac{2h^2(ab\lambda\nu)}{(2j_b + 1)} \frac{2}{E_0 - |\epsilon_a - \epsilon_F| - |\epsilon_b - \epsilon_F| - \hbar\omega_{\lambda\nu}}, \quad (60)$$

in which E_0 is the pairing energy per Cooper pair (equal to about -2Δ) [8]. This expression was inserted in the BCS gap equation, without taking explicitly into account the renormalization effects on the single-particle density, namely, setting the N and Z factors equal to one, and using a mean-field potential characterized by an effective mass $m^* = m$. One then

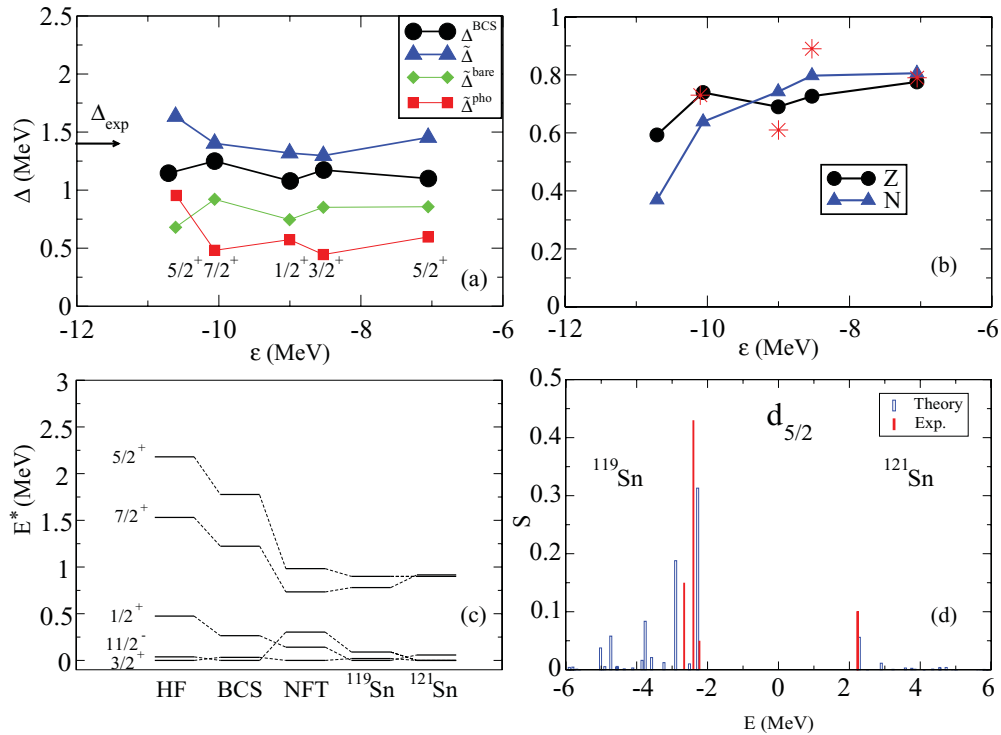


FIG. 15. (Color online) Results obtained solving the Nambu-Gor'kov equations including the coupling to spin modes with the SLy4 mean field, shifting the energy of the $d_{5/2}$ orbital by 600 keV toward the Fermi energy: (a) renormalized gaps, (b) Z and N factors, (c) quasiparticle spectrum, (d) $5/2^+$ strength function.

found gaps about 20% larger than those obtained solving the Nambu-Gor'kov equations [9,10]. The simplified expression for V_{ind} was also employed in a more elaborate calculation [13], which used HF levels calculated with the SLy4 interaction and a constant value $N = 0.7$. However, $\tilde{\Sigma}_{12}$ was identified with the pairing gap, which then tended to be overestimated by a factor $1/Z$.

B. Summary of the main results

In Fig. 15, we show the results of a calculation with the bare pairing interaction, including all the elements discussed in the previous sections. The calculation is analogous to that reported in Figs. 6–10, but the effect of spin modes has been included, and the energy of the unperturbed $d_{5/2}$ orbital in the SLy4 mean field has been shifted.

The spectroscopic factors and the induced pairing gap are not much affected by the details of the mean field or of the effective mass associated with the effective forces we have examined (cf. the Appendix). These quantities are essentially determined by the interweaving with low-lying collective surface vibrations, which shifts the quasiparticle energies, increasing the level density close to the Fermi energy, and leads to spectroscopic factors (Z and N factors) in the range 0.6–0.8 [cf. Fig. 15(b)] and to an induced pairing gap $\tilde{\Delta}^{\text{pho}}$ of about 0.8 MeV. The coupling of spin modes, owing to their higher energy and smaller collectivity, is likely not to affect much the spectroscopic results. With our very simple estimates we find that this coupling reduces the induced pairing gap by about 0.2 MeV, leading to a final induced pairing gap $\tilde{\Delta}^{\text{pho}}$ close to 0.6 MeV [cf. Fig. 15(a)].

The calculated strength function of fragmented levels lying not far from the Fermi surface (the $d_{5/2}$ in the present case) depends on the detailed position of the levels in the mean-field potential, and the comparison with experiment provides important information on it. In particular, we have shifted the position of the $d_{5/2}$ orbital in the SLy4 mean field by about 600 keV, to improve the agreement with the observed strength function [cf. Fig. 15(d), to be compared with Fig. 10].

We find that the calculated total pairing gap $\tilde{\Delta}$ provides an overall account of the value derived from the experimental odd-even mass difference. Starting from the value $\Delta^{\text{BCS}} = 1.1$ MeV obtained with the value of m_k associated with the SLy4 interaction [cf. Fig. 15(a)]. In fact, $\tilde{\Delta} = \tilde{\Delta}^{\text{pho}} + \Delta^{\text{BCS}} \times Z = 0.6$ MeV + 0.8 MeV = 1.4 MeV.

We remark that microscopic pairing forces lead to a weak state dependence for the orbitals close to the Fermi energy, so that in this region we obtain essentially the same results—both at the BCS level and after the renormalization process—with a simple monopole interaction, using a suitable value of the pairing constant (cf. Fig. 24 in the Appendix). Furthermore, different values of Δ^{BCS} , associated with different momentum dependences of m_k far from the Fermi energy, essentially lead to a shift of the final gap $\tilde{\Delta}$, but do not alter significantly the spectroscopic results shown in Figs. 15(b)–15(d) (cf. Figs. 24–26 in the Appendix). It is of notice that a conclusive theoretical calculation of m_k is not yet available.

IV. CONCLUSIONS

We have discussed in detail a well-known formalism to deal with the basic renormalization processes induced by

the coupling between quasiparticle and collective vibrations in superfluid spherical nuclei. We have solved the Nambu-Gor'kov equations determining the normal and abnormal energy-dependent self-energies self-consistently. This allows for a calculation of the low-energy part of the nuclear spectrum in odd nuclei taking into account the fragmentation of the quasiparticle strength, as well as the calculation of the pairing gap of the system including the pairing interaction induced by the exchange of collective modes. The mean field is based on a HF calculation with the effective SLy4 interaction, while the coupling between quasiparticles and vibrations is determined by a QRPA calculation that reproduces the empirical polarizability of the low-lying vibrational modes.

We emphasize several points which are novel as compared to previous work.

- (i) We have derived a gap equation [cf. Eqs. (38) and (43)] that takes into account renormalization effects in a compact way, distinguishing the role of the normalization factors and extending previous expressions by including the contribution of the energy dependent induced interaction.
- (ii) We have introduced two different calculational schemes depending on whether the bare pairing interaction and the renormalization effects are taken into account simultaneously (one-step diagonalization) or sequentially (two-step diagonalization), performing first a BCS calculation with the bare force. We have shown (cf. the Appendix) that the two schemes lead to similar results for states close to Fermi energy in the case of a simple monopole pairing force with a realistic coupling strength. The two-step scheme is computationally much simpler in the case of realistic nucleon-nucleon forces which can scatter particles to very high energies.
- (iii) Last but not least, we have stressed the importance of a global analysis of the quasiparticle properties that includes on the same footing energies, spectroscopic factors, and pairing gaps. Only by comparing all these quantities with the experimental findings does it become possible to make a meaningful comparison between different theoretical schemes and to appreciate the full importance of medium polarization effects.

The formalism allows also for a clear separation between the contribution of the bare force and of renormalization effects: Their contributions to the pairing gap turn out to be of similar magnitude, confirming previous studies.

From our results, summarized in Sec. III B, we conclude that it is possible, at least in the case of ^{120}Sn , to draw a picture that is consistent with the available experimental data concerning the quasiparticle properties close to the Fermi energy. The results appear to be stable with respect to reasonable changes in the ingredients of our calculations (cf. the Appendix).

Several elements remain to be further investigated, before one can reach firm quantitative theoretical results, in particular concerning the absolute value of the total pairing gap. On the one hand, the mean field should be either derived microscopically [78], or at least refitted comparing theory and experiment taking into account renormalization effects;

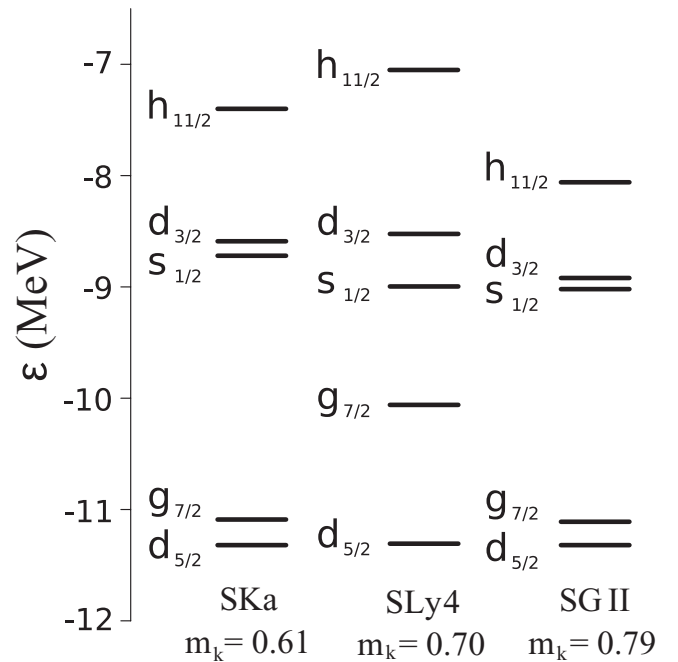


FIG. 16. Energies of the five HF single-particle levels lying close to the Fermi energy in ^{120}Sn , calculated with the effective interactions SKa, SLy4, and SGII. The effective mass associated with these forces at saturation density is also indicated.

on the other hand, contributions that are expected to provide a repulsive contribution to the pairing interaction, associated with three-body effects and with the influence of spin modes, have started only recently to be examined.

ACKNOWLEDGMENTS

Most of the work reported in this paper has been carried out in close collaboration with R. A. Broglia. F.B. acknowledges financial support from the Ministry of Science and Innovation of Spain grants FPA2009-07653, ACI2009-1056 and FIS2011-28738-C02-01.

APPENDIX

In this Appendix we consider the sensitivity of our results to some of the prescriptions and ingredients of the calculations.

1. Mean field

The results obtained in the main text have been obtained with a HF mean field produced by the SLy4 interaction, whose effective mass at saturation is $m_k = 0.7m$. In this section we show results obtained with two different interactions of the Skyrme type: the SKa [80] and the SGII [81], having respectively a lower ($m_k = 0.61m$) and a larger ($m_k = 0.78m$) effective mass. All the other features of the calculations are the same as for SLy4. In particular, the particle-vibration matrix elements are the same, because in our approach they only depend on the properties of the phenomenological phonons and are calculated with the wave functions of a fixed potential with effective mass equal to one. As expected, the SGII interaction

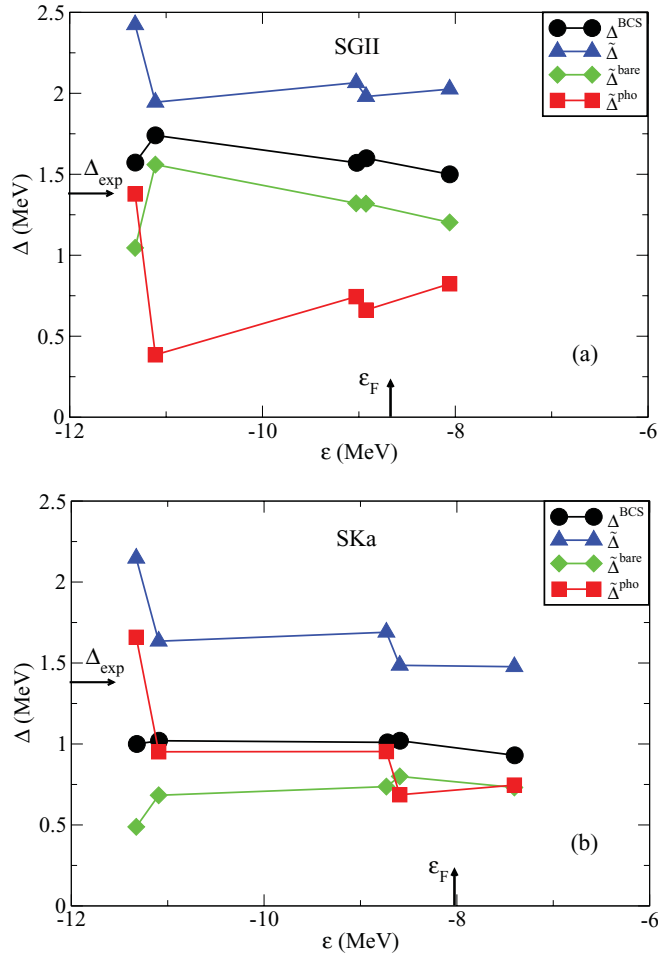


FIG. 17. (Color online) The state-dependent pairing gap Δ^{BCS} calculated in BCS with the bare v_{14} interaction is compared to the renormalized gap $\tilde{\Delta}$ [cf. Eq. (38)] obtained solving the Nambu-Gor'kov equations. We compare results obtained with a mean field produced with the SGII interaction (a) and with the SKa interaction (b) (cf. Fig. 6 for the corresponding calculation with the SLy4 mean field) [79]. The symbols refer to the position of the various valence orbitals in the SGII HF potential. We also show the decomposition of $\tilde{\Delta}$ into the bare and phonon contributions $\tilde{\Delta}^{\text{bare}}$ and $\tilde{\Delta}^{\text{pho}}$. The value of the Fermi energy ϵ_F and of the gap obtained from the experimental odd-even mass difference Δ_{exp} are also indicated.

produces a mean field associated with a higher level density, leading to a larger pairing gap in the BCS calculation with the v_{14} potential, as shown in Fig. 17(a): The value of Δ^{BCS} is equal to about 1.6 MeV, to be compared with the value 1.1 MeV previously obtained with the SLy4 interaction (cf. Fig. 6(a)). The value obtained with the SKa interaction is instead equal to about 1 MeV [cf. Fig. 17(b)].

The renormalization processes act in a very similar way, as was previously found in the case of SLy4. The average value of the phonon induced gap $\tilde{\Delta}^{\text{pho}}$ is in all cases equal to about 0.8 MeV: In the case of SGII $\tilde{\Delta}^{\text{pho}}$ accounts for about 30% of the total gap, while in the case of SKa $\tilde{\Delta}^{\text{pho}}$ and $\tilde{\Delta}^{\text{bare}}$ are of similar magnitude, as in the case of SLy4.

The low-lying spectra are shown in Fig. 18, while the Z and N factors of the lowest fragments are reported in Fig. 19.

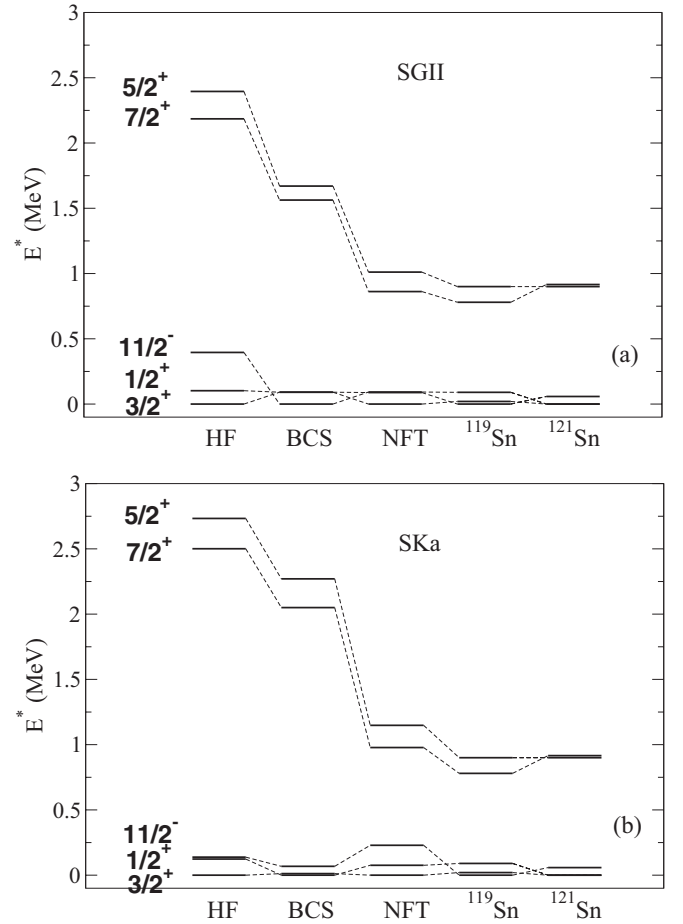


FIG. 18. The theoretical quasiparticle spectra obtained at the various steps of the calculation are compared to the experimental data. We compare results obtained with a mean field produced with the SGII interaction (a) and with the SKa interaction (b) (cf. Fig. 8 for the corresponding calculation with the SLy4 mean field).

Also in this case, medium renormalization effects are similar to those already discussed in the case of the SLy4 interaction (cf. Fig. 7 and Fig. 8). However, the agreement with experiment is better than obtained previously. This is attributable to the initial position of the $d_{5/2}$ and $g_{7/2}$ orbitals, which are closer to each other; furthermore, the $d_{5/2}$ single-particle calculated with SGII lies at a distance of about 2.2 MeV from the Fermi energy, instead of 2.8 MeV as in the case of SLy4: This leads to a good description of the fragmentation of this orbital, as shown in Fig. 20, that in the case of SLy4 was obtained only shifting the energy of this level (cf. Figs. 10 and 15(d)). The quality of the quasiparticle spectrum obtained with SKa is almost as good as with SGII; however, the orbital $g_{7/2}$ lies more distant from the Fermi energy and becomes fragmented, contrary to experiment (the calculated value of $N_{g_{7/2}}$ is about 0.35, cf. Fig. 19). It is interesting to notice that taking the SLy4 mean field, and changing the energies of the five valence orbitals with those associated with the SGII interaction, one obtains practically the same spectrum and the same Z and N factors as with SGII. This in spite of the fact that Δ^{BCS} becomes equal to about 1.25 MeV, to be compared with 1.1 MeV (SLy4) and 1.6 MeV (SGII). At the same time, the average value of

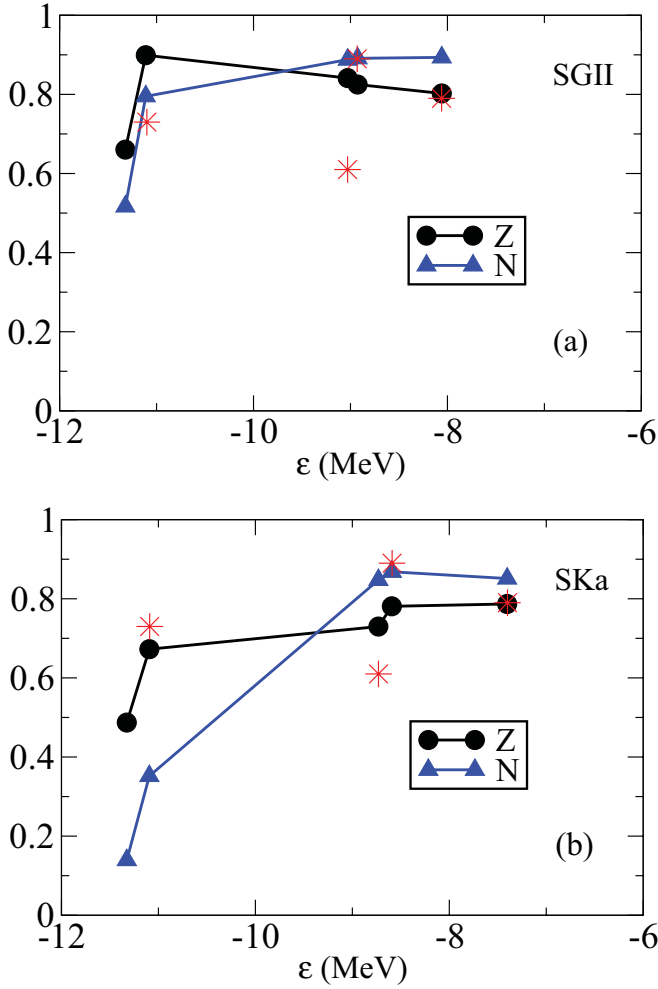


FIG. 19. (Color online) Comparison of the N and Z factors associated with the lowest quasiparticle peaks in the Nambu-Gor'kov calculation shown in Fig. 17. We compare results obtained with a mean field produced with the SGII interaction (a) and with the SKa interaction (b) (cf. Fig. 7 for the corresponding calculation with the SLy4 mean field). Also shown by stars are the values of the experimental quasiparticle strength [66], except for the $d_{5/2}$ orbital, which shows a pronounced fragmentation.

$\tilde{\Delta}$ is equal to about 1.7 MeV, to be compared with 1.6 MeV (SLy4) and 2.1 MeV (SGII) (cf. Fig. 21). These results show that the low-energy spectrum is determined by the position of the valence orbitals, while the absolute value of the gaps also depends on the effective mass associated with distant levels.

We can conclude that renormalization effects are similar for the three mean fields we have considered. The comparison with the odd-even mass difference favors forces having low effective mass (SLy4 or SKa). Renormalization effects improve the agreement of the spectral properties with experiment. However, the quality of this agreement depends on the specific position of the mean-field single-particle levels close to the Fermi energy. The value of the effective mass far from the Fermi energy affects the magnitude of the final gap $\tilde{\Delta}$ by shifting the value of Δ^{BCS} , while the value of $\tilde{\Delta}^{\text{pho}}$ and the properties of the low-lying spectrum are not very sensitive to it.

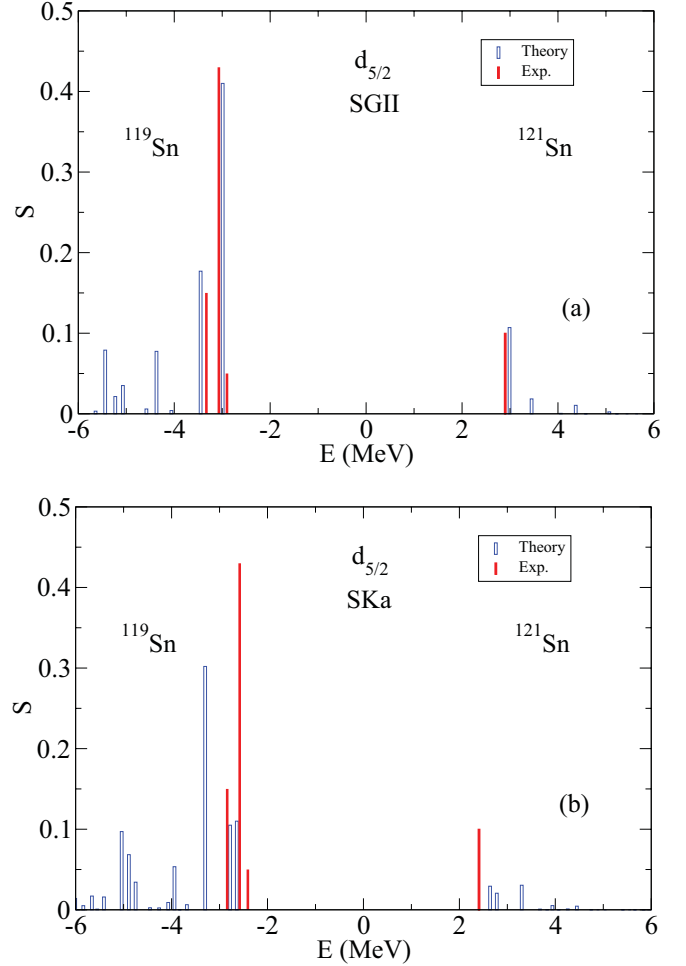


FIG. 20. (Color online) The theoretical strength function calculated for the $d_{5/2}$ orbital is compared to the spectroscopic factors associated with experimental levels detected in one-neutron transfer reactions. We compare results obtained with a mean field produced with the SGII interaction (a) and with the SKa interaction (b) (cf. Fig. 10 for the corresponding calculation with the SLy4 mean field).

2. Bare pairing interaction

The calculations reported in the main text have been carried out adopting v_{14} as the bare pairing force. However, the V_{lowk} version of the Argonne potential has been used by several groups and here we show the results using this bare pairing force in our Nambu-Gor'kov formalism. The corresponding bare and renormalized gap are shown in Fig. 22. The average value of the bare gap is equal to about 1.4 MeV, in agreement with Ref. [61], to be compared with the value 1.1 MeV obtained with the Argonne interaction. The effect of the renormalization processes increases the gap on average by about 500 keV, similar to the case of v_{14} (600 keV, cf. Fig. 6). Also the values of the phonon-induced component $\tilde{\Delta}^{\text{pho}}$ are quite similar. The results of the calculations with v_{14} and V_{lowk} turn out to be quite similar to those obtained using the monopole force respectively with coupling constants $G_0 = 0.22$ and $G_0 = 0.25$ MeV (cf. Fig. 26).

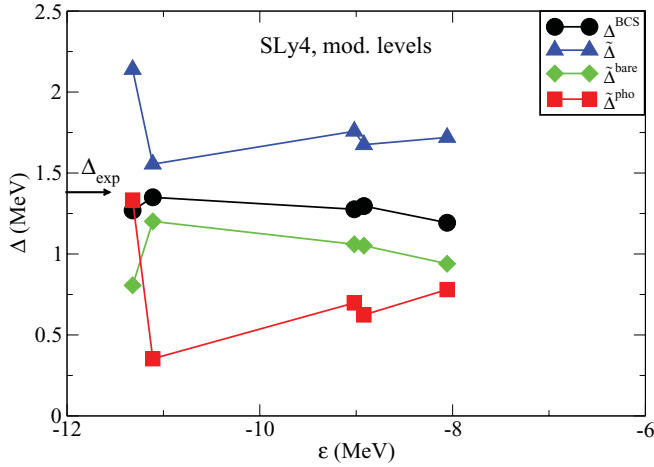


FIG. 21. (Color online) The same as in Fig. 17, for the pairing gaps calculated with the SLy4 mean field, but substituting the single-particle energies of the five valence orbitals with the energies calculated in the SGII mean field.

3. QRPA

We recall (cf. Sec. II) that the results shown in the main text are based on effective particle-vibration vertices calculated with single-particle levels and wave function associated with a Woods-Saxon potential, with an associated effective mass $m^* = m$. Another reasonable choice, often adopted in the literature, would be to use instead the same single-particle levels used in the HF + BCS calculation. Using this prescription and readjusting the coupling constants χ_λ of the QRPA calculation so as to reproduce the experimental properties of the low-lying vibrational states, we obtain the renormalized pairing gaps shown in Fig. 23. It is seen that the difference is not critical, because our preferred choice leads to gaps which are smaller by only about 10%.

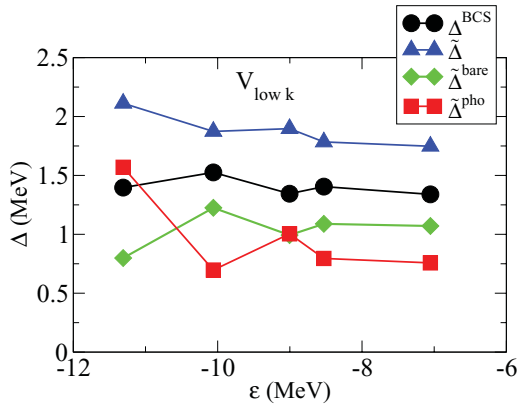


FIG. 22. (Color online) The state-dependent pairing gap Δ^{BCS} calculated using the $V_{\text{low}k}$ potential with a cutoff $\Lambda = 4 \text{ fm}^{-1}$ as pairing force is compared to the renormalized gap $\tilde{\Delta}$ [cf. Eq. (38)] obtained solving the Nambu-Gor'kov equations. The symbols refer to the position of the various valence orbitals in the SLy4 HF potential. We also show the decomposition of $\tilde{\Delta}$ into the bare and phonon contributions $\tilde{\Delta}^{\text{bare}}$ and $\tilde{\Delta}^{\text{pho}}$. We thank A. Pastore for providing us with the HFB calculation with the $V_{\text{low}k}$ potential.

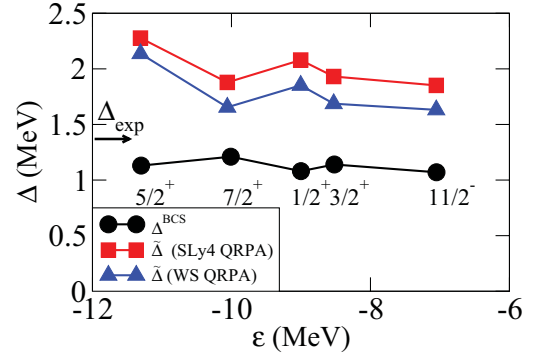


FIG. 23. (Color online) The renormalized pairing gap $\tilde{\Delta}$, calculated using the levels of a Woods-Saxon potential to compute the QRPA spectrum and the particle-vibration vertices, is shown by triangles (cf. Fig. 6) and is compared to the results obtained using SLy4 single-particle levels (squares). We also show the pairing gap Δ^{BCS} calculated in BCS (dots).

4. Comparison of the one-step and two-step diagonalization schemes with the monopole pairing force

Solving the Nambu-Gor'kov equations in the one-step diagonalization scheme is numerically very demanding in the case of realistic nucleon-nucleon interactions. In this appendix we want to compare the one-step and the two-step diagonalization schemes using a simple monopole pairing force, $-G_0 P^\dagger P$ acting only in our valence space. The present calculation is similar to that presented in Ref. [9], except for

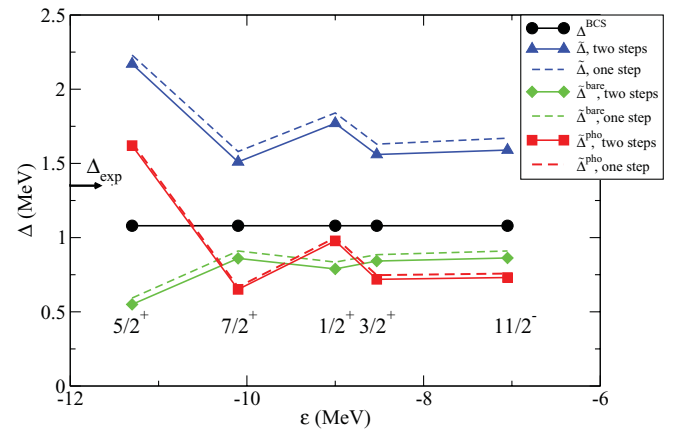


FIG. 24. (Color online) Comparison of the renormalized pairing gaps $\tilde{\Delta}$ associated with the lowest energy fragments, obtained solving the Nambu-Gor'kov equations in the two-step (solid line with triangles) and the one-step diagonalization (dashed line) schemes. We also show the bare ($\tilde{\Delta}^{\text{bare}}$) and the phonon ($\tilde{\Delta}^{\text{pho}}$) components of the renormalized gaps in the two-step diagonalization (solid lines with diamonds and squares) and the one-step diagonalization (dashed lines) schemes. The pairing interaction is a monopole force with coupling constant $G_0 = 0.22 \text{ MeV}$, acting in the valence shell around the Fermi energy in ^{120}Sn , which produces the gap Δ^{BCS} (solid lines with dots) obtained in the BCS calculation. The symbols refer to the position of the various valence orbitals in the SLy4 HF potential. The value of the gap Δ_{exp} obtained from the experimental odd-even mass difference is also indicated.

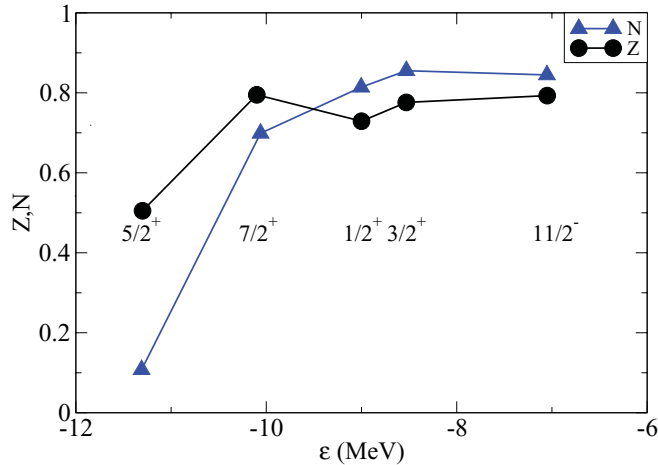


FIG. 25. (Color online) Z and N factors associated with the various valence orbitals, for the calculation presented in Fig. 24. The values obtained in the one-step and the two-step diagonalizations are indistinguishable on the scale of the figure.

details in the mean field (here obtained from a SLy4 interaction instead of a Woods Saxon potential with effective mass $m^*=0.7$), in the QRPA spectrum and in the determination of the particle-vibration coupling. We, however, present new results that will extend our previous investigation.

In Fig. 24 we compare the results obtained in the one- and the two-step schemes, for a value $G_0 = 0.22$ MeV, corresponding to a bare pairing gap $\Delta^{\text{BCS}} = 1.08$ MeV. We have chosen this particular value of G_0 to reproduce the average value of the gap Δ^{BCS} obtained previously with the v_{14} interaction (cf. Fig. 6(a)). We see that the renormalized pairing gaps are very similar in the one-step and the two-step diagonalization schemes. Moreover, the results are also similar to those obtained with the Argonne interaction, shown in Fig. 6(b), not only for the total gap $\tilde{\Delta}$ but also concerning the decomposition into bare and phonon contribution. The similarity extends also to the Z and N factors, shown in Fig. 25 (cf. Fig. 7). The fact that the results turn out to be close to those obtained using the Argonne interaction is easy to understand in the two-step diagonalization scheme, which is based on the quasiparticle and occupation amplitudes obtained with the bare interaction. In fact, the realistic nucleon-nucleon interaction displays a limited state dependence over the valence orbitals, with an average value $\Delta^{\text{BCS}} = 1.1$ MeV.

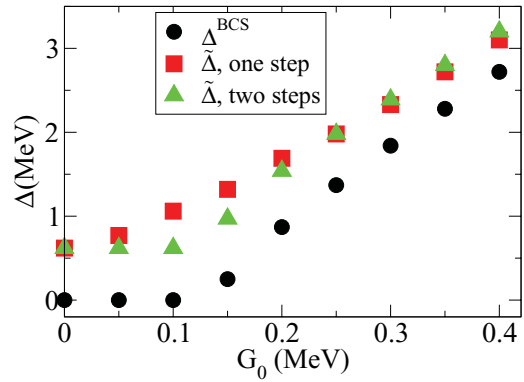


FIG. 26. (Color online) Renormalized gaps $\tilde{\Delta}$ obtained solving the Nambu Gor'kov equations in the one-step and the two-steps diagonalization schemes with the monopole pairing force as a function of the pairing constant G_0 , averaged over the five valence orbitals. Also shown is the gap Δ^{BCS} obtained solving the BCS equation.

In Fig. 26 we show the value of the gap, averaged over the five valence orbitals, as a function of the pairing strength G_0 . In the two-step diagonalization scheme, one starts from the u_a, v_a amplitudes obtained in a previous BCS calculation with the bare force, which for G_0 smaller than 0.1 MeV produces no superfluid solution. However, the induced interaction V_{ind} is able to produce a pairing gap by itself. As a consequence, in the two-step diagonalization scheme only $\tilde{\Sigma}_{\text{phon}}^{12}$ contributes to the gap, which is therefore underestimated and independent of G_0 for $G_0 < 0.1$. Instead, using the one-step diagonalization scheme, the gap grows as a function of G_0 because the bare interaction can provide a contribution to pairing correlations even for small values of G_0 when it is added to the induced interaction through the effective interaction $V_{\text{eff}} = V_{\text{bare}} + V_{\text{ind}}$. For values of G_0 larger than 0.1 MeV, the gaps in the one-step and the two-step diagonalization scheme become closer and closer, until the two-step diagonalization scheme becomes satisfactory for values of the order of $G_0 = 0.2$ MeV. It is interesting to note that the calculations for the bare and renormalized gaps performed with $G_0 = 0.25$ MeV reproduce quite well the results obtained using the $V_{\text{low}k}$ interaction as bare pairing force (cf. Fig. 22). This indicates that Fig. 26 can be used to assess in a simple way the effect of renormalization processes on pairing correlations for the adopted QRPA spectrum.

- [1] P. F. Bortignon, R. A. Broglia, D. R. Bes, and R. Liotta, *Phys. Rep.* **C 30**, 305 (1977).
- [2] C. Mahaux, P. F. Bortignon, R. A. Broglia, and C. H. Dasso, *Phys. Rep.* **120**, 1 (1985).
- [3] V. G. Soloviev, *Theory of Atomic Nuclei. Quasiparticles and Nuclei* (Institute of Physics Publishing, Bristol, Philadelphia, 1992).
- [4] L. P. Gor'kov, *Sov. Phys. JETP* **7**, 505 (1958).
- [5] Y. Nambu, *Phys. Rev.* **117**, 648 (1960).

- [6] G. M. Eliashberg, *Sov. Phys. JETP* **11**, 696 (1960).
- [7] G. Potel, A. Idini, F. Barranco, E. Vigezzi, and R. A. Broglia, [arXiv:0906.4298](https://arxiv.org/abs/0906.4298) [nucl-th].
- [8] F. Barranco, R. A. Broglia, G. Gori, E. Vigezzi, P. F. Bortignon, and J. Terasaki, *Phys. Rev. Lett.* **83**, 2147 (1999).
- [9] J. Terasaki, F. Barranco, R. A. Broglia, E. Vigezzi, and P. F. Bortignon, *Nucl. Phys. A* **697**, 127 (2002).
- [10] J. Terasaki, F. Barranco, R. A. Broglia, E. Vigezzi, and P. F. Bortignon, *Progr. Theor. Phys.* **108**, 495 (2002).

- [11] F. Barranco, R. A. Broglia, G. Colò, E. Vigezzi, and P. F. Bortignon, *Eur. Phys. J. A* **21**, 57 (2004).
- [12] F. Barranco, P. F. Bortignon, R. A. Broglia, G. Colò, P. Schuck, E. Vigezzi, and X. Viñas, *Phys. Rev. C* **72**, 054314 (2005).
- [13] A. Pastore, F. Barranco, R. A. Broglia, and E. Vigezzi, *Phys. Rev. C* **78**, 024315 (2008).
- [14] D. R. Bes, R. A. Broglia, G. G. Dussel, R. J. Liotta, and H. M. Sofia, *Nucl. Phys. A* **260**, 1 (1976).
- [15] P. F. Bortignon, R. A. Broglia, D. R. Bes, and R. Liotta, *Phys. Rep. C* **30**, 305 (1977).
- [16] A. Bohr and B. R. Mottelson, *Nuclear Structure* (Benjamin, San Francisco, 1975), Vol. II.
- [17] D. R. Bes, R. A. Broglia, G. G. Dussel, R. J. Liotta, and H. M. Sofia, *Nucl. Phys. A* **260**, 27 (1976).
- [18] P. F. Bortignon and R. A. Broglia, *Nucl. Phys. A* **371**, 405 (1981).
- [19] G. F. Bertsch, P. F. Bortignon, and R. A. Broglia, *Rev. Mod. Phys.* **55**, 287 (1983).
- [20] R. A. Broglia, F. Barranco, G. Colò, G. Gori, and E. Vigezzi, in *Proceedings of the International School of Physics "Enrico Fermi,"* Course CLIII, edited by A. Molinari, L. Riccati, W. M. Alberico, and M. Morando, p. 65 (IOS Press, Amsterdam, 2003).
- [21] C. Barbieri and W. H. Dickhoff, *Phys. Rev. C* **65**, 064313 (2002).
- [22] C. Barbieri and W. H. Dickhoff, *Phys. Rev. C* **68**, 014311 (2003).
- [23] C. Barbieri and M. Hjorth-Jensen, *Phys. Rev. C* **79**, 064313 (2009).
- [24] V. Somà, T. Duguet, and C. Barbieri, [arXiv:1109.6230](https://arxiv.org/abs/1109.6230).
- [25] E. V. Litvinova and A. V. Afanasjev, *Phys. Rev. C* **84**, 014305 (2011).
- [26] G. Colò, H. Sagawa, and P. F. Bortignon, *Phys. Rev. C* **82**, 064307 (2010).
- [27] A. Ansari and P. Ring, *Phys. Rev. C* **74**, 054313 (2006).
- [28] J. Terasaki, J. Engel, and G. F. Bertsch, *Phys. Rev. C* **78**, 044311 (2008).
- [29] W. H. Dickhoff and D. Van Neck, *Many-Body Theory Exposed! Propagator Description of Quantum Mechanics in Many-body Systems*, 2nd ed. (World Scientific, Singapore, 2008).
- [30] V. Van der Sluys, D. Van Neck, M. Waroquier, and J. Ryckebusch, *Nucl. Phys. A* **551**, 210 (1993).
- [31] J. R. Schrieffer, *Superconductivity* (Benjamin, San Francisco, 1964).
- [32] R. A. Broglia, O. Hansen, and C. Riedel, *Adv. Phys.* **6**, 287 (1973).
- [33] A. Bohr and B. R. Mottelson, *Nuclear Structure* (Benjamin, San Francisco, 1969), Vol. I.
- [34] D. Rowe, *Nuclear Collective Motion* (Methuen, London/New York, 1970).
- [35] C. Bloch and Horowitz, *Nucl. Phys.* **8**, 91 (1958).
- [36] S. T. Belyaev and V. G. Zelevinskii, *Sov. J. Nucl. Phys.* **1**, 10 (1965).
- [37] A. V. Avdeenkov and S. P. Kamerdzhev, [arXiv:nucl-th/0111072](https://arxiv.org/abs/nucl-th/0111072).
- [38] V. A. Khodel, *Phys. Rep.* **92**, 183 (1983).
- [39] F. Barranco and R. A. Broglia, *Phys. Rev. Lett.* **59**, 2724 (1987).
- [40] V. A. Khodel, A. P. Platonov, and E. E. Saperstein, *J. Phys. G* **8**, 967 (1982).
- [41] S. A. Fayans, S. V. Tolokonnikov, E. L. Trykov, and D. Zawischa, *Nucl. Phys. A* **676**, 49 (2000).
- [42] F. Barranco and R. A. Broglia, *Phys. Lett. B* **151**, 90 (1985).
- [43] J. I. Escudero, F. Barranco, and G. Madurga, *J. Phys. G* **13**, 1261 (1987).
- [44] S. Kamerdzhev and E. E. Saperstein, *Eur. Phys. J. A* **37**, 333 (2008).
- [45] A. V. Avdeenkov and S. P. Kamerdzhev, *Phys. At. Nucl.* **62**, 563 (1999).
- [46] A. V. Avdeenkov and S. P. Kamerdzhev, *Phys. Lett. B* **459**, 423 (1999).
- [47] F. Barranco, P. F. Bortignon, R. A. Broglia, G. Colò, and E. Vigezzi, *Eur. Phys. J. A* **11**, 385 (2001).
- [48] G. Gori, F. Barranco, E. Vigezzi, and R. A. Broglia, *Phys. Rev. C* **69**, 041302(R) (2004).
- [49] U. Lombardo, P. Schuck, and W. Zuo, *Phys. Rev. C* **64**, 021301(R) (2001).
- [50] M. Baldo and A. Grasso, *Phys. Lett. B* **485**, 115 (2000).
- [51] S. Baroni, A. O. Macchiavelli, and A. Schwenk, *Phys. Rev. C* **81**, 064308 (2010).
- [52] D. Van Neck, M. Waroquier, and J. Ryckebusch, *Nucl. Phys. A* **530**, 347 (1991).
- [53] D. Van Neck, M. Waroquier, V. Van der Sluys, and J. Ryckebusch, *Nucl. Phys. A* **563**, 1 (1993).
- [54] O. Beer, A. El Behay, P. Lopato, Y. Terrien, G. Vallois, and Kamal K. Seth, *Nucl. Phys. A* **147**, 326 (1970).
- [55] F. Barranco, R. A. Broglia, H. Esbensen, and E. Vigezzi, *Phys. Lett. B* **390**, 13 (1997).
- [56] P. M. Pizzochero, F. Barranco, E. Vigezzi, and R. A. Broglia, *Astrophys. J.* **569**, 381 (2002).
- [57] P. Ring and P. Schuck, *The Nuclear Many-body Problem* (Springer-Verlag, New York, 1980).
- [58] E. Chabanat, P. Bonche, P. Haensel, J. Meyer, and R. Schaeffer, *Nucl. Phys. A* **635**, 231 (1998).
- [59] N. Fotiadis, R.O. Nelson, M. Devlin, and J.A. Becker, *Phys. Rev. C* **76**, 014302 (2007).
- [60] G. Colò, S. Fracasso, and P. F. Bortignon, *Phys. Lett. B* **646**, 227 (2007).
- [61] K. Hebeler, T. Duguet, T. Lesinski, and A. Schwenk, *Phys. Rev. C* **80**, 044321 (2009).
- [62] M. Baldo, U. Lombardo, S. S. Pankratov, and E. E. Saperstein, *J. Phys. G* **37**, 064016 (2010).
- [63] W. Zuo, U. Lombardo, H.-J. Schulze, and C. W. Shen, *Phys. Rev. C* **66**, 037303 (2002).
- [64] T. Duguet, T. Lesinski, K. Hebeler, and A. Schwenk, *Mod. Phys. Lett.* **25**, 1989 (2010).
- [65] T. Duguet, T. Lesinski, K. Hebeler, and A. Schwenk, [arXiv:1104.2955](https://arxiv.org/abs/1104.2955) [nucl-th].
- [66] S. A. Dickey, J. J. Kraushaar, R. Ristinen, and M. A. Rumore, *Nucl. Phys. A* **377**, 137 (1982).
- [67] M. Bender, K. Rutz, P.-G. Reinhard, and J. A. Maruhn, *Eur. Phys. J. A* **8**, 49 (2000).
- [68] T. Duguet, P. Bonche, P.-H. Heenen, and J. Meyer, *Phys. Rev. C* **65**, 014311 (2001).
- [69] F. Barranco, R. A. Broglia, H. Esbensen, and E. Vigezzi, *Phys. Lett. B* **390**, 13 (1997).
- [70] E. Gerlic, G. Berrier-Ronsin, G. Duhamel, S. Galès, E. Hourani, H. Langevin-Joliot, M. Vergnes, and J. Van de Wiele, *Phys. Rev. C* **21**, 124 (1980).
- [71] M. J. Bechara and O. Dietzsch, *Phys. Rev. C* **12**, 90 (1975).
- [72] K. Moghrabi, M. Grasso, G. Colò, and N. Van Giai, *Phys. Rev. Lett.* **105**, 262501 (2010).
- [73] J. M. C. Chen, J. W. Clark, R. D. Davé, and V. V. Khodel, *Nucl. Phys. A* **555**, 59 (1993).
- [74] J. Wambach, T. Ainsworth, and D. Pines, *Nucl. Phys. A* **555**, 128 (1993).
- [75] H.-J. Schulze, J. Cugnon, A. Lejeune, M. Baldo, and U. Lombardo, *Phys. Lett. B* **375**, 1 (1996).

- [76] H. Heiselberg, C. J. Pethick, H. Smith, and L. Viverit, *Phys. Rev. Lett.* **85**, 2418 (2000).
- [77] G. Gori, F. Ramponi, F. Barranco, P. F. Bortignon, R. A. Broglia, G. Colo, and E. Vigezzi, *Phys. Rev. C* **72**, 011302 (2005).
- [78] H. Hergert and R. Roth, *Phys. Rev. C* **80**, 024312 (2009).
- [79] L. Micene, Master's thesis, University of Milano, 2007.
- [80] H. Köhler, *Nucl. Phys. A* **258**, 301 (1976).
- [81] N. van Giai and H. Sagawa, *Phys. Lett. B* **106**, 379 (1981).